

## 2. EXPLANATORY NOTES<sup>1</sup>

### Shipboard Scientific Party<sup>2</sup>

#### INTRODUCTION

In this chapter, we have assembled information that will help the reader understand the observations on which our preliminary conclusions are based and also help the interested investigator select samples for further analysis. This information concerns only shipboard operations and analyses described in the site reports in the Leg 174A *Initial Reports* volume of the *Proceedings of the Ocean Drilling Program*.

#### Authorship of Site Chapters

The separate sections of the site chapters were written by the following shipboard scientists (authors are listed in alphabetical order, no seniority is implied):

Site Summary: Austin, Christie-Blick  
Background and Objectives: Austin, Christie-Blick  
Operations: Austin, Malone, Pollard  
Lithostratigraphy: Berné, Damuth, Hesselbo, Hoyanagi, Krawinkel, McHugh, Savrda, Sohl, Vanderaveroet  
Biostratigraphy: Katz, McCarthy, Olson, Smart, Wei  
Paleomagnetism: Oda  
Organic Geochemistry: Claypool, Dickens  
Inorganic Geochemistry: Dickens, Malone  
Physical Properties: Borre, Fulthorpe, Whiting  
Downhole Logging: Delius, Flemings, Major, Mountain, Pirmez  
Seismic Stratigraphy: Austin, Christie-Blick, Mountain  
Summary and Conclusions: Austin, Christie-Blick

Summary core descriptions and photographs of each core are included in Section 3, this volume. Smear-slide and thin-section descriptions, large data sets, and logging figures processed postcruise are on CD-ROM located in the back pocket of the volume.

#### Shipboard Scientific Procedures

Core handling and shipboard scientific procedures—including the numbering of sites, holes, cores, sections, and samples—are similar to those reported in previous *Initial Reports* volumes of the *Proceedings of the Ocean Drilling Program* (e.g., Shipboard Scientific Party, 1995a).

At the end of the leg, the cores were transferred from the ship in refrigerated airfreight containers to cold storage at the East Coast Repository of the Ocean Drilling Program (ODP) at Lamont-Doherty Earth Observatory. Investigators interested in obtaining samples should contact the Science Operator.

#### LITHOSTRATIGRAPHY

This section outlines the procedures followed to document the basic sedimentology of the cores recovered during Leg 174A, including

core description, sediment classification, X-ray diffraction analysis, color spectrophotometer measurements, and smear-slide and thin-section preparation.

#### Visual Core Description

##### *Barrel Sheets*

Information from visual description of each core was recorded manually for each section on paper core-description forms. This information was then condensed and entered into AppleCORE (v0.7.5d) software to generate a simplified, one-page graphical description of each core (barrel sheet). Barrel sheets are presented with whole-core photographs in Section 3 (in black and white) and on CD-ROM (in color), back pocket of this volume.

The lithology of each core is represented on barrel sheets by graphic patterns in the column on the left side of the sheet (Fig. 1). The sediments recovered from the New Jersey shelf generally contain small percentages of microscopic biogenic particles (e.g., nannofossils, foraminifers, diatoms, radiolarians, and sponge spicules) dispersed in siliciclastic muds and sands of variable texture. Grain-size divisions for sand, silt, and clay are those of Wentworth (1922); “mud” is used here in the sense of a mixture of silt and clay (discussed below). Each sediment type is represented by a single siliciclastic-sediment pattern if it is homogeneous in texture (e.g., sand) or by two patterns, if two texturally distinct siliciclastic sediments are interbedded (e.g., interbeds of sand and silty clay; Fig. 2). The width of each column indicates the relative proportion of each type of siliciclastic sediment in the interbedded interval. Alternatively, in a less accurate but more realistic portrayal, interbedded lithology may be shown by intercalation of this pattern with others. Minor constituents (<10%) of a certain lithology are indicated in the “Description” section of the barrel sheet.

A wide variety of features that characterize the sediment, such as bioturbation parameters, primary sedimentary structures, soft-sediment deformation, structural features, diagenetic phenomena (accessories), ichnofossils, and core disturbance, are indicated in columns to the right of the graphic log (Fig. 1). The symbols are schematic and are placed as closely as possible to their proper stratigraphic position; exact positions of sedimentary features are shown in the detailed section-by-section paper core-description forms at ODP. A key to the full set of symbols used on the graphic sedimentologic columns is shown in Figure 1. The sample column shows locations for samples taken from each core and includes SS = smear slide, IW = interstitial water, HS = headspace (organic geochemistry), PAL = paleontology, and DCP = detailed core photo.

Bed thickness is characterized as very thick bedded (>100 cm thick), thick bedded (30–100 cm thick), medium bedded (10–30 cm thick), thin bedded (3–10 cm thick), and very thin bedded (1–3 cm thick; McKee and Weir, 1953). The hue and chroma attributes of color, as determined visually using Munsell Soil Color Charts (Munsell, 1990), are recorded in the “Description” column.

Deformation and disturbance of sediment that clearly resulted from the coring process are illustrated in the “Drilling Disturbance” column, using symbols shown in Figure 1. Blank regions indicate an absence of coring disturbance. Detailed accounts of drilling disturbance appear in many previous ODP reports (e.g., Shipboard Scientific Party, 1995b).

<sup>1</sup>Austin, J.A., Jr., Christie-Blick, N., Malone, M.J., et al., 1998. *Proc. ODP, Init. Repts.*, 174A: College Station, TX (Ocean Drilling Program).

<sup>2</sup>Shipboard Scientific Party is given in the list preceding the Table of Contents.

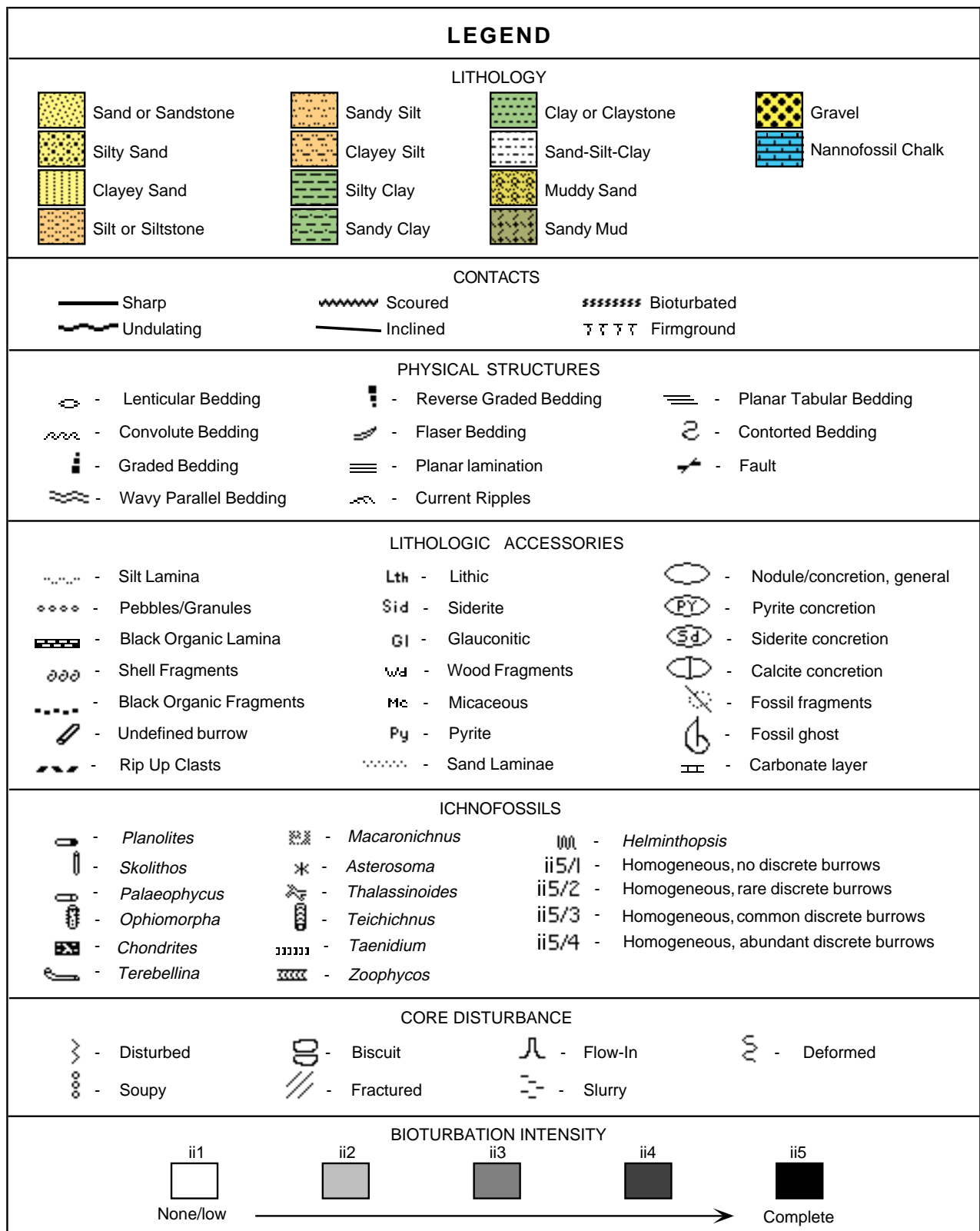


Figure 1. Key to symbols used to represent lithology, contacts, sedimentary structures, trace fossils, diagenetic components, and drilling disturbance in the barrel sheets contained in Figure 4 of the “Site 1071” chapter, Figure 3 of the “Site 1072” chapter, and in Section 3 (all in this volume).

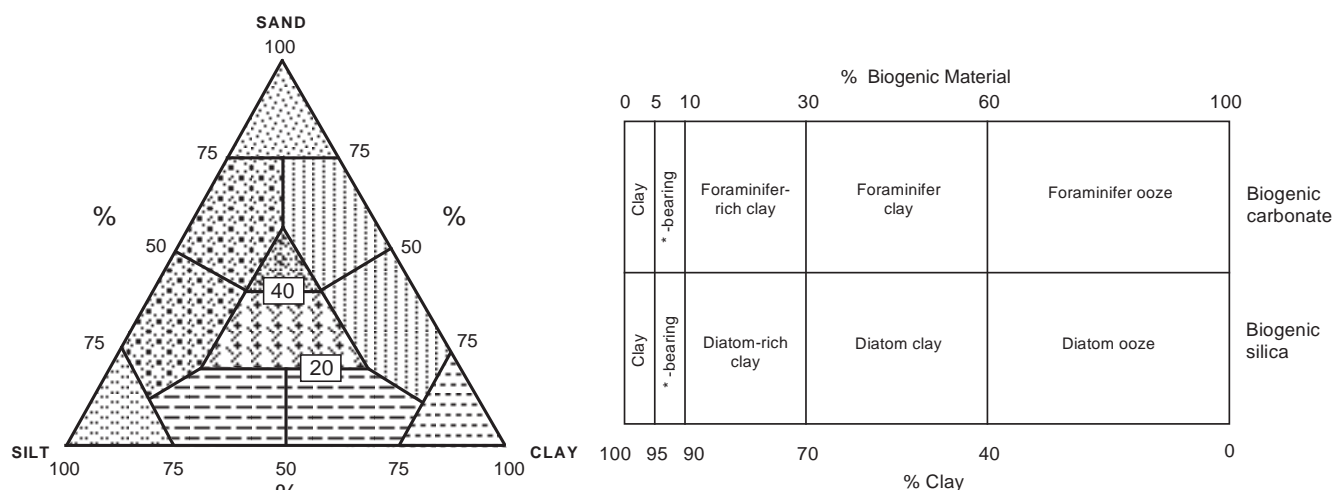


Figure 2. Textural classification scheme for siliciclastic sediments (left), and the procedure for naming mixtures of biogenic and siliciclastic materials (right). The textural classification scheme is modified from Shepard (1954) by subdivision of the central triangular field into muddy sand and sandy mud. The sand-, silt-, and clay-sized fractions are defined using the Wentworth (1922) grade scale. Symbols on the Shepard triangle are the same as shown in Figure 1. In the scheme for biogenic-siliciclastic mixtures, the names for microfossil components and the siliciclastic fraction are examples only (i.e., placeholders) and can be replaced by any valid textural name (for siliciclastic fraction) or microfossil name. Examples are foraminifer silty clay and nannofossil-rich sandy mud. The asterisks in the scheme for biogenic-clastic mixtures indicate an unusual component, such as plant debris, present in amounts of 5%–10%; use of this “-bearing” category is optional.

A summary lithologic description with sedimentologic highlights is given in the “Remarks” column of the barrel sheet. This generally consists of four parts: (1) a section that lists all the major sediment lithologies; (2) a section for minor lithologies; (3) an extended summary description of the sediments, including color, composition, sedimentary structures, trace fossils identified, and other notable characteristics; and (4) chronostratigraphic units identified by shipboard paleontologists and paleomagnetists. Descriptions and locations of thin, interbedded, or minor lithologies that could not be depicted in the graphic lithology column are presented in the Remarks column, where space permits.

### Sediment Classification

The sediment classification scheme used during Leg 174A is descriptive and is largely the same as previously used by ODP (Fig. 2). Composition and texture are the only criteria used to define lithology. Genetic terms such as pelagic, hemipelagic, turbidite, debris flow, etc., do not appear in this classification. The term “clay” is used for both clay minerals and other siliciclastic material <4  $\mu\text{m}$  in size. Biogenic components are not described in textural terms. Thus, a sediment with 55% sand-sized foraminifers and 45% siliciclastic clay is called a foraminifer clay, not a foraminifer clayey sand.

The principal name is determined by the component or group of components (e.g., total biogenic carbonate) that compose(s) at least 60% of the sediment or rock, except for subequal mixtures of biogenic and nonbiogenic material. If the total of a nonbiogenic component is >60%, the main name is determined by the relative proportions of sand, silt, and clay sizes when plotted on a modified Shepard (1954) classification diagram (Fig. 2). Examples of nonbiogenic principal names are clay, silt, silty clay, or sand. If the total of biogenic components is >60%, the principal name is ooze.

In mixtures of biogenic and nonbiogenic material where the biogenic content is 30%–60%, the principal name consists of two parts: (1) the name of the major fossil(s), hyphenated if necessary with the least common fossil listed first, followed by (2) the textural name appropriate for the siliciclastic components. In cases of subequal mixtures of calcareous microfossils, the modifiers “calcareous” or “carbonate-rich” can be used instead of microfossil names (Fig. 2).

If a component represents 10%–30% of a sediment, it qualifies for minor modifier status and is hyphenated with the word “rich,” such as nannofossil-rich clay. If a component composes only 5%–10% of sediment, but is nonetheless deemed of significance (e.g., plant material, granules, sand), it can be indicated with a minor modifier that consists of the component name hyphenated with the word “bearing” (Fig. 2). Examples are plant-bearing clay and sand-bearing silty clay. This is an optional modifier. The most abundant accessory component appears closest to the principal name. Major and minor modifiers are listed in order of decreasing abundance to the left of the principal name.

Example: foraminifer-rich nannofossil clay  
(10%) (35%) (55%)

Chemical sediments and diagenetic beds or nodules, including minerals formed by inorganic precipitation such as evaporites and many carbonates, are classified according to mineralogy, texture, and fabric. For lithified sediments, the suffix “stone” is added to the principal names of sand, silt, clay, or mud. The term “chalk” is used for partially lithified sediment composed of >60% calcareous nannofossils.

### Ichnology

Ichnologic analysis included evaluation of the extent of bioturbation, as well as identification of trace-fossil types. To assess the degree of bioturbation semiquantitatively, a modified version of the Droser and Bottjer (1991) ichnofabric index (ii1 to ii5) scheme was employed (e.g., ii1 = barren or no bioturbation, ii5 = abundant bioturbation or homogeneous; Fig. 3). These indices are illustrated using color-banded symbols in the “Relative Bioturbation” column of the barrel sheets. For completely bioturbated sediments (ii = 5), ichnofabrics were assessed using a modified version of the “slash” scheme of Droser and Bottjer (1991) in an attempt to distinguish homogeneous or diffusely burrow-mottled backgrounds from discrete biogenic structures (e.g., ii5/4 refers to completely bioturbated background fabrics heavily overprinted by discrete ichnofossils; Fig. 3). Slash indices were depicted in the “Ichnofossils” column of the barrel

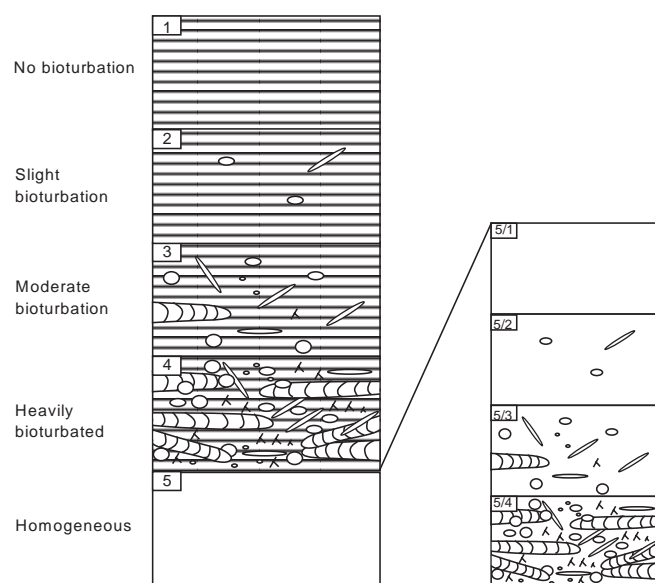


Figure 3. Key to ichnofabric index used during Leg 174A (modified from Droser and Bottjer [1991] by the deletion of category 6).

sheets (using symbols shown in Fig. 1). Interpretation of completely homogeneous sediments presented some problems. Where such fabrics were attributed to primary deposition, ii1 was assigned. Where these fabrics were interpreted to reflect total biogenic mixing, they were assigned to ii5/1.

Trace-fossil identification was restricted to intervals wherein biogenic structures were discrete, such as where burrows exhibited sharp walls or had fills that contrasted well (in texture, composition, or color) with surrounding sediments. Discrete biogenic structures (e.g., burrows, burrow systems, and borings) were identified on the basis of morphologic attributes as manifested on two-dimensional core surfaces. Recognizable biogenic structures are illustrated in the Ichnofossils column of barrel sheets, using symbols depicted in Figure 1.

### X-ray Diffraction

Relative abundances of the main silicate and carbonate minerals were determined semiquantitatively using a Philips Model PW-1729 X-ray diffractometer with Cu K $\alpha$  radiation (Ni filter). Each bulk-sediment sample was freeze-dried, crushed, and mounted with a random orientation into an aluminum sample holder. Instrument settings were 40 kV, 35 mA, goniometer scan from 2° to 70° 2 $\theta$  for bulk samples, step-size 0.01° 2 $\theta$ , scan speed at 1.2° 2 $\theta$ /min, and count time 0.5 s. Peak intensities were converted to values appropriate for a fixed slit width. An interactive software package (MacDiff 3.2b5 PPC) was used on a Macintosh computer to identify the main minerals and to measure peak areas. Relative abundances of various minerals were established on the basis of integrated peak intensity. The locations of the peaks used for mineral recognition are presented in Table 1. Ratios and relative abundances reported in this volume are useful for general characterization of the sediments, but should not be viewed as precise quantitative data.

### Smear Slides

Petrographic analysis of sediments was primarily by smear-slide description. Tables summarizing data from smear slides appear on CD-ROM (back pocket, this volume). These tables include information about the sample location, whether the sample represents a dominant (D) or a minor (M) lithology in the core, and the estimated per-

**Table 1. Positions of diagnostic peaks used for the identification of minerals in X-ray diffractograms and for quantification of peak intensities.**

Mineral	Peak-2 $\theta$ (°)	Peak-Å
Quartz	26.65	3.34
K-feldspars	26.93-27.52	3.31-3.24
Plagioclases	27.77-28.13	3.21-3.17
Hornblende	10.30-10.70	8.59-8.27
Calcite	29.45	3.03
Dolomite	30.94	2.89
Pyrite	33.05	2.71
Siderite	32.07	2.79
Opal-CT	21.94-21.67	4.05-4.10
Clinoptilolite	9.83	8.99

Note: Opal-A shows a very broad peak around 4Å.

centage ranges of sand, silt, and clay, together with all identified components. We emphasize here that smear-slide analysis provides only crude estimates of the relative abundances of detrital constituents. The mineral identification of finer grained particles is difficult using only a binocular microscope, and sand-sized grains tend to be underestimated because they cannot be incorporated into the smear evenly. The mineralogy of smear-slide components was validated by X-ray diffraction.

### Thin Sections

Thin sections of lithified sediments were made by impregnation under vacuum with Epo-tek resin as needed. Thin sections were stained with alizarin red for determination of calcite and dolomite, and with potassium ferricyanide for identification of iron carbonates.

### Spectrophotometer

Reflectance of visible light from cores was routinely measured using a Minolta Spectrophotometer CM-2002. The purpose was to establish semiquantitative relationships between lithology and spectral reflectance for visible (VIS) wavelengths, to provide a continuous stratigraphic record of color variations downhole, and to try to recognize climatic signals in Pleistocene-age sediments.

Spectrophotometer readings were taken before cleaning the surface of the working half of the cores. Strips of very thin, transparent plastic film (Glad Cling Wrap, a brand of polyethylene food wrap) were used to cover the cores to prevent the spectrophotometer from becoming dirty. Routine measurements were generally made at evenly spaced intervals of each core section, normally 10 or 30 cm, but interval spacing was sometimes modified according to section length and void distribution. The measurement spacing was reduced to <10 cm for some cored intervals wherein distinct, fine-scale color variations or changes in lithology occurred throughout short distances, and for intervals where climatic signals were to be investigated.

Before obtaining measurements from each core, the spectrophotometer was calibrated by attaching its white calibration cap (the white calibration cap was not covered with plastic food wrap because the Minolta instrument receives calibration values from the white cap; see Balsam et al., 1997). The spectrophotometer measurements were then recorded using the program Spectrolog (v 3.0). Each measurement consists of 31 separate determinations of reflectance in 10-nm-wide spectral bands from 400 to 700 nm, which covers the VIS spectrum. Additional detailed information about measurement and interpretation of spectral data with the Minolta spectrophotometer can be found in Schneider et al. (1995) and Balsam et al. (1997).

### BIOSTRATIGRAPHY

Preliminary age assignments were established using core-catcher (CC) samples. Samples from elsewhere in the cores were examined

when a more refined age determination was necessary and when time permitted. Three microfossil groups were examined for biostratigraphic purposes: calcareous nannofossils, planktonic foraminifers, and dinoflagellate cysts (dinocysts). Benthic foraminifers were used to estimate paleobathymetry and to establish preliminary paleoenvironment and provenance interpretations. Sample positions and the abundance, preservation, and chronostratigraphic age or biozone for benthic and planktonic foraminifers, as well as a subset of the dinoflagellates, were recorded in the ODP JANUS database. The Cenozoic time scale used in this work is from Berggren et al. (1995; Fig. 4). Table 2 summarizes the planktonic foraminifer datum levels used for Leg 174A.

### Foraminifers

#### Methods

Samples of ~20 cm<sup>3</sup> were soaked in a Calgon solution, washed through a 63- $\mu$ m sieve, and dried under a heat lamp.

Preservation characteristics were divided into four categories:

- P (poor) = almost all specimens were dissolved or broken and fragments dominated;
- M (moderate) = 30%–60% of specimens showed dissolved or broken chambers;
- G (good) = 60%–90% of specimens were well preserved and unbroken; and
- VG (very good) = >90% of specimens were well preserved and unbroken.

#### Planktonic Foraminifers

The Cenozoic zonal schemes of Berggren et al. (1995) were used in this study (Fig. 4) and supplemented by information from Kennett and Srinivasan (1983). Where possible, the equivalent zonal schemes of Blow (1969) are referred to in this study to enable comparison of Leg 174A planktonic foraminifer data with zonal schemes from previous scientific ocean drilling legs. Biostratigraphic datums used for the Cenozoic are shown in Table 2.

The >125- $\mu$ m fraction was examined for planktonic foraminifers, and the 63- to 125- $\mu$ m fraction was studied for zonal markers if they were absent in the larger size fractions. In many samples, abundances were so low that quantitative counts of individual species were recorded. In cases where abundances were higher, qualitative counts were made by estimating the percentage of the planktonic foraminifer fauna as follows:

- B (barren) = none;
- P (present) = <1%;
- R (rare) = 1%–4%;
- F (few) = 5%–9%;
- A (abundant) = 10%–30%; and
- D (dominant) = >30%.

In addition, the planktonic/benthic ratio for each sample was estimated.

Neogene taxonomic concepts follow Kennett and Srinivasan (1983) and Chaisson and Leckie (1993). In general, taxonomic nomenclature follows that used by Berggren et al. (1995).

#### Benthic Foraminifers

Benthic foraminifers were examined from the >150- $\mu$ m-size fraction. Species abundance relative to the total benthic foraminifer fauna was estimated as follows:

- B (barren) = none;
- R (rare) = <1%;
- F (few) = 1%–4%;

- C (common) = 5%–20%; and
- A (abundant) = >20%.

Bathymetric zones were defined as middle bathyal (600–1000 m), upper bathyal (200–600 m), and neritic (0–200 m), which was divided into inner (0–50 m), middle (50–100 m), and outer (100–200 m). Taxonomic concepts, paleobathymetric estimates, and paleoenvironment and provenance interpretations were based on multiple references for the Pleistocene (Buck and Olson, in press; Ellison and Nichols, 1976; Gevirtz, 1971; Loeblich and Tappan, 1953; Murray, 1969; Parker, 1948; Poag et al., 1980; van Morkhoven et al., 1986) and Pliocene–Miocene sections (Cushman and Cahill, 1933; Gibson, 1983; Miller et al., 1997; Olsson et al., 1987; Schnitker, 1970; Snyder et al., 1989; van Morkhoven et al., 1986).

### Calcareous Nannofossils

We have referred primarily to the zonation of Bukry (1973, 1975) as codified by Okada and Bukry (1980). Numerical ages used are those compiled by Berggren et al. (1995) to facilitate easy comparison with other studies. Calcareous nannofossil assemblages were described from smear slides prepared for each CC sample and for as many additional core samples as time permitted. Standard preparation techniques were used throughout. Examination was performed exclusively with a light microscope, using whatever optical configuration yielded useful results. In all cases, a magnification of 1000 $\times$  was used to make semiquantitative estimates of abundances.

Abundances of individual species were estimated for each sample. Five levels of abundance were recorded, with the following approximate definitions:

- R (rare) = 1 specimen per 51 or more fields of view;
- F (few) = 1 specimen per 11–50 fields of view;
- C (common) = 1 specimen per 2–10 fields of view;
- A (abundant) = 1–10 specimens per field of view; and
- V (very abundant) = >10 specimens per field of view.

Total abundance of calcareous nannofossils for each sample was estimated as follows:

- B (barren) = none;
- R (rare) = 1–10 specimens for 500 fields of view (about three traverses);
- F (few) = 11–50 specimens for 500 fields of view;
- C (common) = 51–2,000 specimens for 500 fields of view;
- A (abundant) = 2,001–20,000 specimens for 500 fields of view; and
- V (very abundant) = >20,000 specimens for 500 fields of view.

The qualitative evaluation of the preservation of calcareous nannofossils was recorded as poor (P), moderate (M), or good (G). These categories represent subjective impressions according to the following definitions:

- P (poor) = Severe dissolution, fragmentation, and/or overgrowth have occurred. Primary features may have been destroyed, and many specimens cannot be identified at the species level.
- M (moderate) = Dissolution and/or overgrowth are evident. A significant proportion (up to 10%) of the specimens cannot be identified to species level with absolute certainty.
- G (good) = There is little or no evidence of dissolution and/or overgrowth. Diagnostic characteristics are preserved and nearly all specimens can be identified to species level.

### Dinoflagellates

We employed the dinocyst zonation of de Verteuil and Norris (1996), which was developed for Miocene coastal plain sediments in

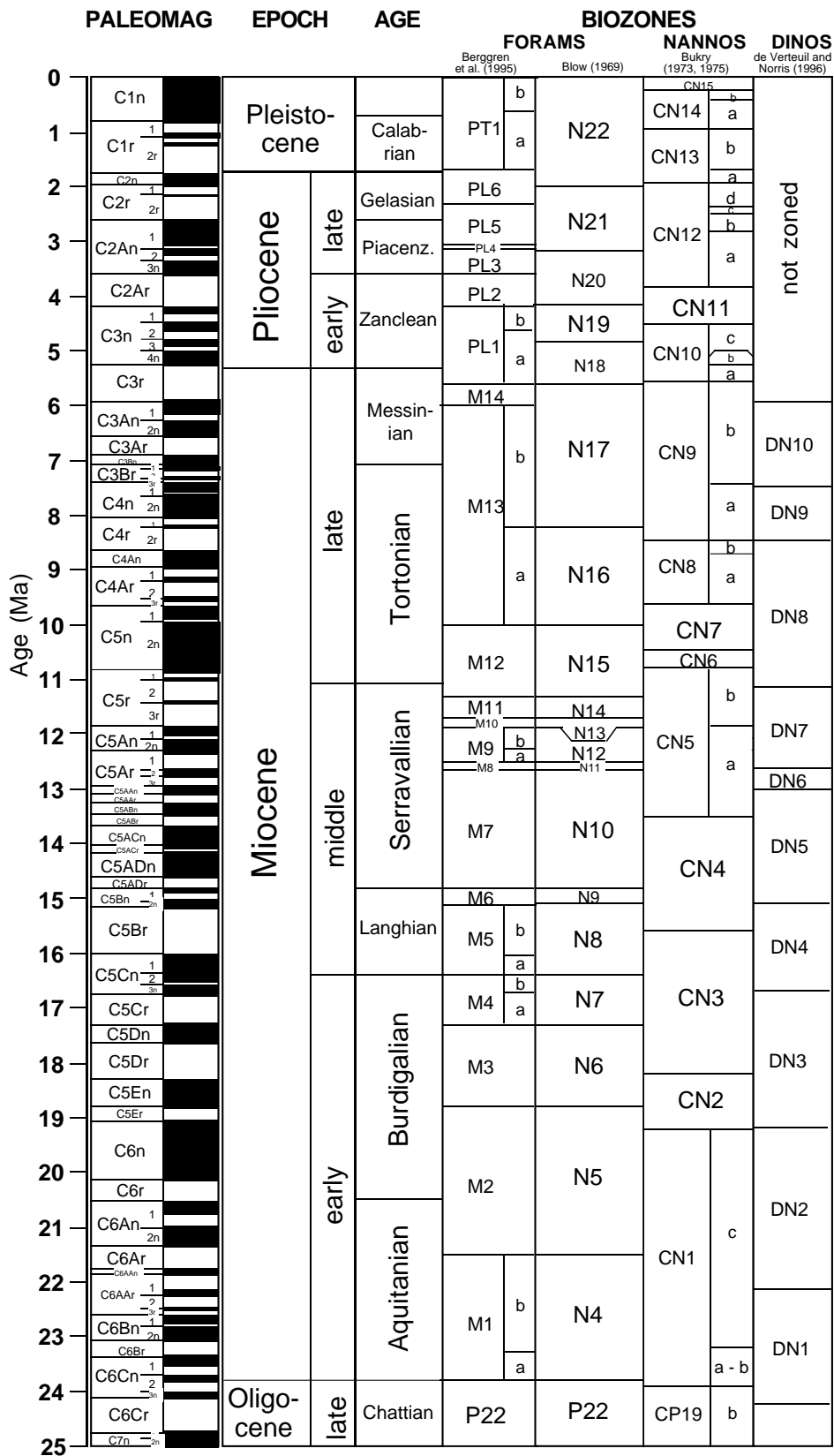


Figure 4. Correlation of Neogene chronostratigraphy, biostratigraphy, and magnetostratigraphy used during Leg 174A. Correlation of the magnetic polarity record and epoch boundaries follows that of Berggren et al. (1995). Estimated numerical ages of planktonic foraminifer zonal indicators can be found in Table 2.

**Table 2. Cenozoic planktonic foraminifer datums used for Leg 174A.**

Event	FO	LO
<i>Turborotalia truncatulinoides</i>	2.00	
<i>Globorotalia inflata</i>	2.09	
<i>Dentoglobigerina altispira</i>		3.09
<i>Globorotalia juanai</i>		4.9
<i>Globoquadrina dehisces</i>		5.8
<i>Globorotalia juanai</i>	8.1	
<i>Candeina nitida</i>	8.1	
<i>Neogloboquadrina pachyderma</i>	9.2	
<i>Neogloboquadrina mayeri</i>		11.4
<i>Paragloborotalia acrostoma</i>		12.5-12.7

Notes: FO = first occurrence, LO = last occurrence. References for age assignments can be found in Berggren et al. (1995). Age range for LO of *Paragloborotalia acrostoma* uses the zonal assignment (N11) of Kennett and Srinivasan (1983).

Maryland, Virginia, and New Jersey and on ODP Leg 150 (New Jersey slope). The zones are calibrated using dinocyst datums established for several sections in the North Atlantic and Europe (summarized in Head et al., 1989). No formal zonation exists for the Pliocene to Holocene on the New Jersey margin. Ages for these sediments are based largely on (1) extensive unpublished data from Deep Sea Drilling Project (DSDP) Site 603 (M.J. Head, pers. comm., 1997), supplemented by magnetostratigraphically constrained datums from DSDP Sites 607 and 611 (Mudie, 1987), and (2) the zonations of Powell (1992) and Harland (1992), which are derived largely from western Europe. Our Paleogene biostratigraphy draws upon dinocyst events in several well-constrained studies, including Head and Norris (1989) and Brinkhuis et al. (1992). These are supplemented by the zonation of Powell (1992), the Northern Hemisphere composite range estimates of Williams et al. (1993), and by studies summarized in Head and Norris (1989).

As many 10-cm<sup>3</sup> CC samples were examined as time permitted. Rarely, additional samples were examined from intervals of particular stratigraphic interest. Processing consisted of heating the sample in 1% Calgon solution, followed by sieving through a 10- $\mu$ m Nitex nylon sieve. Residues were then digested in 20% hydrochloric acid and washed with distilled water. Because of high silica content, samples were digested for 15–20 min in hot concentrated hydrofluoric acid and again washed with water. This was followed by a second application of 20% hydrochloric acid in a hot bath to dissolve precipitated fluorides. Swirling the organic residues in a large watchglass removed residual silicates, sulfides, and detrital minerals when they were present. Residues were strew-mounted on glass slides in glycerine jelly and examined in bright field transmitted light.

Only presence/absence data are available for most samples, and no attempts were made to estimate species abundances except to note where certain taxa clearly dominate an assemblage.

The qualitative evaluation of the preservation of dinocysts only is recorded as poor (P), moderate (M), or good (G). These categories represent subjective impressions with approximately the following meaning:

P (poor) = Severe bacterial infestation, chemical oxidation, and/or mechanical fragmentation have occurred. Primary features were destroyed, and many specimens cannot be identified to the species level.

M (moderate) = Bacterial infestation, chemical oxidation, and/or mechanical fragmentation are evident. Up to 25% of the specimens cannot be identified to species level with certainty.

G (good) = Little or no evidence exists of bacterial infestation, chemical oxidation, or mechanical fragmentation; essentially all (>95%) specimens can be identified to the species level.

All assemblages recovered are thermally immature, and therefore, thermal alteration is not a relevant factor in fragmentation or color alteration of palynomorphs.

## PALEOMAGNETISM

Paleomagnetic studies conducted during Leg 174A consisted of measurements of natural remanent magnetization (NRM) and magnetic susceptibility of sediments. Remanent magnetization measurements were performed both on archive-half sections and oriented cube samples taken from working-half sections using an automated, pass-through cryogenic superconducting DC-SQUID rock magnetometer (2G Enterprises Model 760-R) with an in-line alternating field (AF) demagnetizer (2G Enterprises Model 2G600) that is capable of reaching peak fields of 80 mT with a 200-Hz frequency.

For archive-half samples, the NRM and remanence measurements after AF demagnetization were routinely conducted at 3- or 5-cm intervals starting 10 cm above each core section top and ending as much as 10 cm below each core section bottom. The archive half was mostly demagnetized at 10- and 20-mT increments, and discrete samples at 0, 5, 10, 15, 20, 30, 40, 60, and 80 mT.

The magnetic susceptibility was measured for each whole-core section as part of the multisensor track (MST) (see "Physical Properties" section, this chapter). The MST susceptibility meter (a Bartington MS2C meter with an 88-mm coil diameter and a 0.565-kHz frequency) was set on SI units, and the values were stored in the JANUS database in raw meter units. To convert to true SI-volume susceptibilities, these should first be multiplied by 10<sup>-5</sup>, and then by a correction factor to take into account the volume of material that is passed through the susceptibility coils. Except for measurements near the ends of each section, this factor is ~0.66 (= 1/1.5) for a standard Ocean Drilling Program (ODP) core. Although the plastic core liner was not filled completely in some cases, MST susceptibilities in "Paleomagnetism" sections in the site chapters of this volume are converted into SI units without considering the end effects. Volume susceptibilities of discrete cube samples (7 cm<sup>3</sup>) were measured with a second Bartington Instruments magnetic susceptibility meter (model MS2C).

### Magnetic Field in the Magnetometer

The residual magnetic field inside the pass-through cryogenic magnetometer system was measured several times during Leg 174A (Fig. 5). The magnetic field at the center of the SQUID pick-up coil was <40 nT, whereas that for the center of the AF demagnetizer was <20 nT on 20 June 1997 (crosses; transit from Halifax). At the junction of the mu-metal shields of different diameters, the residual magnetic field is higher than elsewhere. The magnetic field at the junction between the AF demagnetizer and the low field region (smaller diameter mu-metal shield) is around 500 nT, fluctuating with the heading and condition of the ship. The magnetic field at the junction between the SQUID and the AF demagnetizer was higher, up to 9000 nT; however, the field was reduced to ~500 nT by winding a new field cancellation coil with 33 turns outside the shield at the junction and applying a DC current of ~240 mA. The magnetic field measured on 11 July 1997 (solid circles; Fig. 5) is considerably larger than that measured on 20 June (crosses; Fig. 5). The magnetic field inside the cryogenic magnetometer on 11 July was similar to previous measurements; however, the field in the AF demagnetizer was about three times larger than before. On 11 July, an electric current of 1.1 A was needed to reduce the residual magnetic field at the junction between the AF demagnetizer and SQUID.

The magnetic field in the pass-through magnetometer was measured at the junction between the cryogenic magnetometer and the AF demagnetizer (200 cm from the mouth of the cryogenic magnetometer, or 234.5 cm from the CCW limit switch) on 20 June (transit from Halifax), and 11–12 July (Site 1071) at various headings (Fig. 6). The magnetic field in +Z direction of the SQUID magnetometer (ship's forward direction) was the strongest among the three axes, and was at a maximum (~31,000 nT; aft direction) when the ship's heading was magnetic south (magnetic north at the site = 13.51°W).

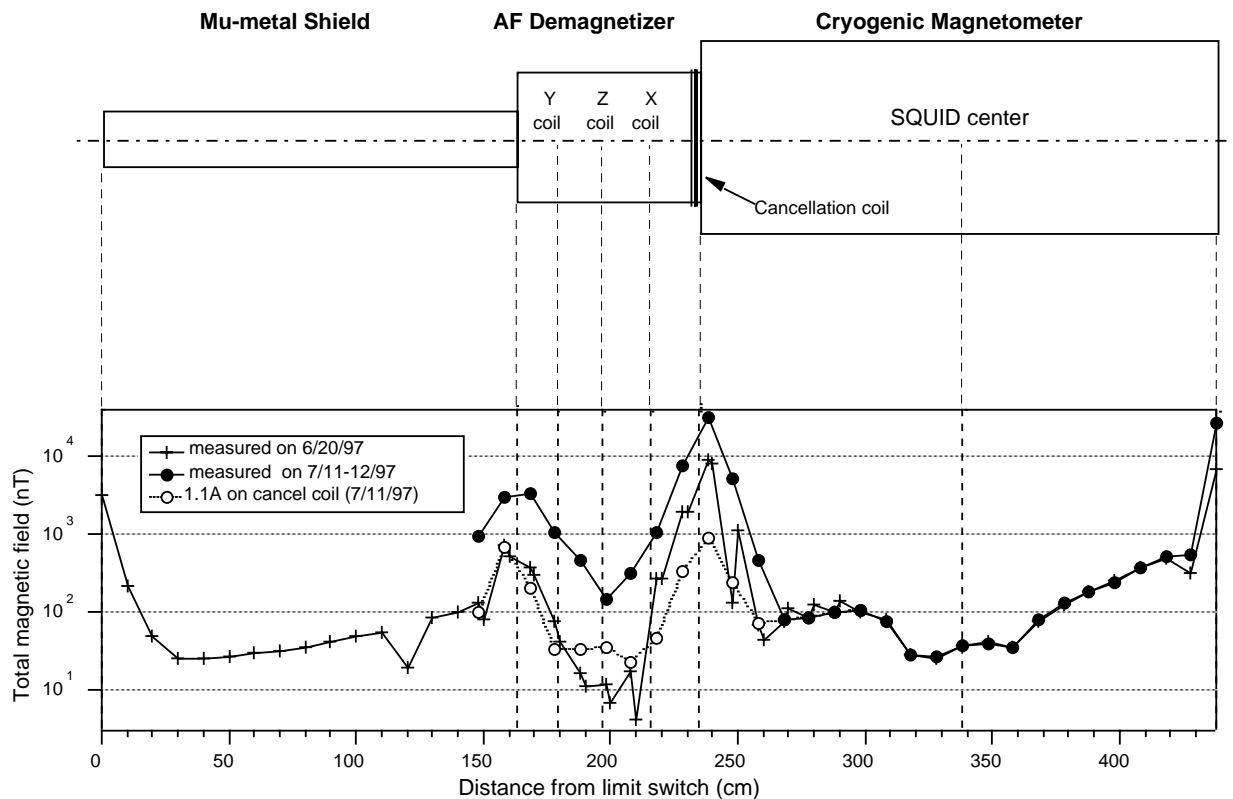


Figure 5. Total magnetic field measured inside the pass-through cryogenic magnetometer system with a fluxgate magnetometer (Applied Physics Systems Model 520).

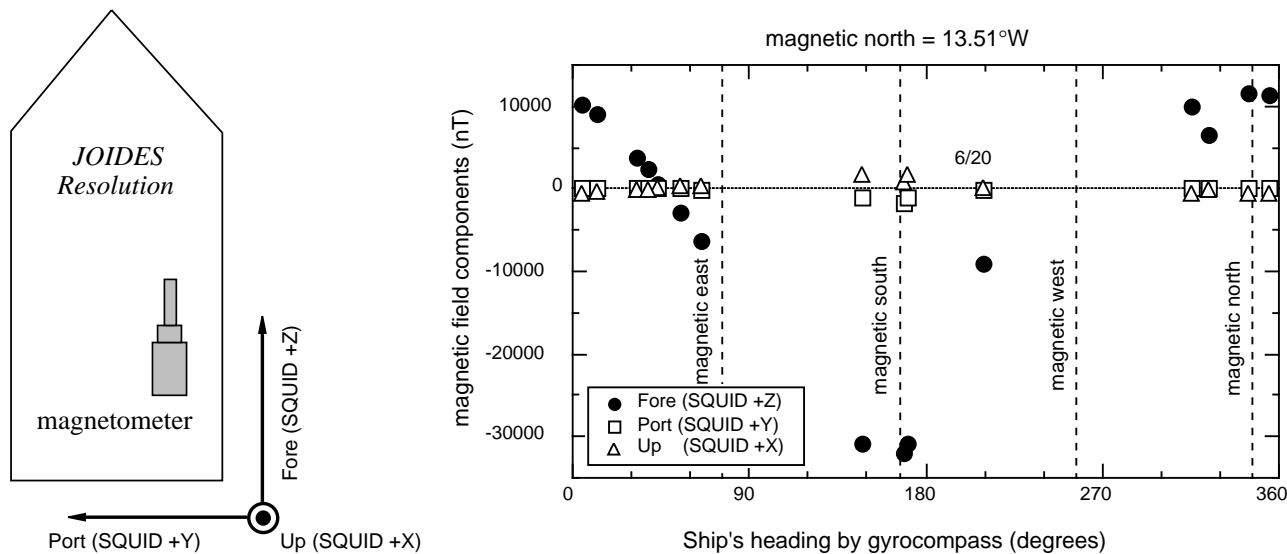


Figure 6. Magnetic field components measured with various ship's headings on 20 June (transit from Halifax), and 11–12 July (Site 1071) of 1997.

The magnetic field intensity came to another local maximum (11,500 nT; forward direction) when the ship's heading was pointing to magnetic north. The asymmetric patterns indicate the presence of a strong permanent magnetization component of the ship. The minimum magnetic field intensity seems to be at ~60° east and 60° west (although there are fewer data points around westerly headings) of magnetic north. The residual magnetic field at the junction of the AF demagnetizer is important, because the magnetic field in some cases may produce anhysteretic remanent magnetization (ARM) at higher magnetic fields, up to 60 mT, as the sample exits the demagnetizing coil during

AF demagnetization (see "Paleomagnetism" section, "Site 1071" chapter, this volume).

### Sampling

The ODP core-orientation scheme arbitrarily designates the positive X-axis direction as the horizontal (in situ north) direction from the center of the core to the median line between a pair of lines inscribed lengthwise on the working half of each core liner (Fig. 7). Discrete samples were taken from the working half using 7-cm<sup>3</sup> ori-

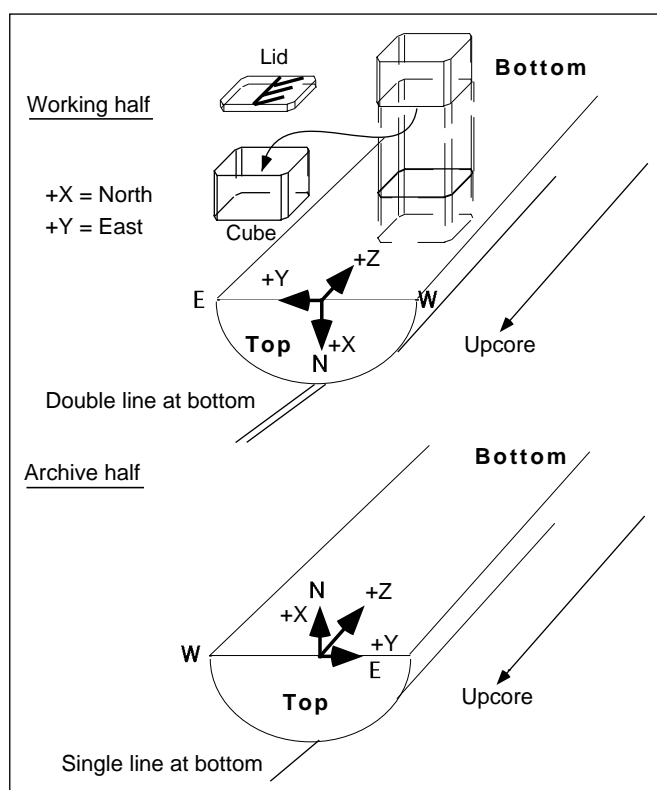


Figure 7. The ODP core orientation scheme arbitrarily designates the positive X-axis direction as the horizontal (in situ north) direction from the center of the core to the median line between a pair of lines inscribed lengthwise on the working half of each core liner. Correspondingly, the negative X-axis direction (in situ south) is the horizontal direction from the center of the core to a median line inscribed lengthwise on the archive half of each core liner.

ented plastic cubes (designed at Kyoto University) and a specially designed stainless steel sampler (Fig. 7).

### Magnetostratigraphy

Where demagnetization successfully isolated the primary component of remanence, paleomagnetic inclinations were used to assign a magnetic polarity to the stratigraphic column. As the Tensor tool in the advanced hydraulic piston corer (APC) was used only at Site 1073 because of operational time constraints, true declination was not available for magnetic polarity determinations at Sites 1071 and 1072. Interpretations of the magnetic polarity stratigraphy, with constraints from the biostratigraphic data, are presented in the site chapters. The revised time scale of Berggren et al. (1995) was used for Cenozoic polarity boundaries.

### Rock Magnetism

The DTECH AF demagnetizer (model D2000) was used for AF-demagnetization experiments on selected discrete samples at higher fields from >80 to 200 mT. The field inside the demagnetizer is typically <50 nT, and the frequency of the alternating field is 116.5 Hz. The demagnetizer was also used to impart ARM on samples in a peak alternating field of 80 mT and a 0.1-mT DC field (79.6 A/m). ARM is carried by relatively fine grains of magnetic minerals, and these are thought to be carriers of stable NRM in most cases. ARM intensity is expressed as susceptibility of ARM ( $K_{arm}$ ) by dividing the ARM by the strength of the biasing DC field.

### Corrections to the Paleomagnetic Data

After Leg 174A (during Leg 176), scientists discovered an error in the cryogenic magnetometer software, which affected ODP Legs 168 through 176. For the paleomagnetism data obtained during Leg 174A, the Y-axis component of the magnetic moment ( $Am^2$ ) and the magnetization (A/m) should be multiplied by  $-1$ . Similarly, the raw declination values should be multiplied by  $-1$ . For the declination values, these calculations result in mirror images with respect to the core north (double fiducial line). All the figures and tables (including tables on CD-ROM) in "Paleomagnetism" sections of this volume should be corrected for y-components of magnetic moments and magnetizations, as well as declination values. In the following section on the sensor-response curves, the sign of the y-component is correct. The magnetic tool face (MTF) angle of the Tensor tool was subtracted from the raw declination values for APC cores at Site 1073 to obtain declinations close to zero for the Brunhes Chron. This procedure resulted in the mirror image of the corrected declination values (Fig. 17, "Site 1073" chapter, this volume). The MTF angle and the raw declination value should be added, as described by Stokking et al. (1993), if the raw declination value is correct.

### Sensor-Response Curve and Deconvolution

The sensor-response curves of the cryogenic magnetometer were measured in the X, Y, and Z directions using a 4-mm plastic cube sample with high coercivity magnetic powder and a magnetic moment of  $7.2 \times 10^{-7} Am^2$  glued in the center (Fig. 8). The standard cube sample was mounted on a vertical plastic plate in 13 different positions (Fig. 8). The sensor-response curves of the standard were measured in the X, Y, and Z directions. The measured sensor responses were integrated over the half-core section to get sensor response for the archive-half samples. The normalized response curves are shown in Figure 9, along with the response curves measured at the position corresponding to the center of the cores (Position 1 in Fig. 8) and 28 mm below the center (Position 2 in Fig. 8). For the sensor response of a half-core sample, normalizations were made with the peak value of a half-core sample in Z axis (ODP half core;  $-Z > Z$ ), whereas normalizations were made with the peak value of z-axis sensor response at the center (ODP Center;  $-Z > Z$ ) for the sensor responses measured at the center and 28 mm below the center.

The half widths of the sensor responses are 7 cm for the X and Y axes and 7.5 cm for the Z axis. These are narrower than ~11 cm measured from the old magnetometer (Oda and Shibuya, 1996). As the radial distance from the center of the pick-up coil increases, the half widths of the response curves become narrower and the peak value increases. The half widths of the sensor-response curves lie between those measured at the center and those measured at 28 mm below the center, due to integration over the cross section of an archive-half sample. The higher peak values at the margin of the pick-up coils and the distortion of the direction of the magnetization due to cross terms (see ODP [0 mm, 28 mm]  $-Z > X$  term in Fig. 9) increase the noise and distort the paleomagnetic signal in the pass-through measurement data of archive-half samples, because the outer parts of the core samples are more disturbed by drilling. The outer, disturbed part has a large volume compared with the central, less disturbed part, which also increases the noise level of the pass-through measurements.

Deconvolution of paleomagnetic data using the sensor-response curves was conducted on pass-through data at Site 1071 using the method of Oda and Shibuya (1996). The spatial resolution of the paleomagnetic signal was enhanced from the original half width of the magnetometer (~7 cm) to ~3 cm after deconvolution.

### INORGANIC GEOCHEMISTRY

Shipboard interstitial water analyses were performed on water squeezed from whole-round sections (Manheim and Sayles, 1974).

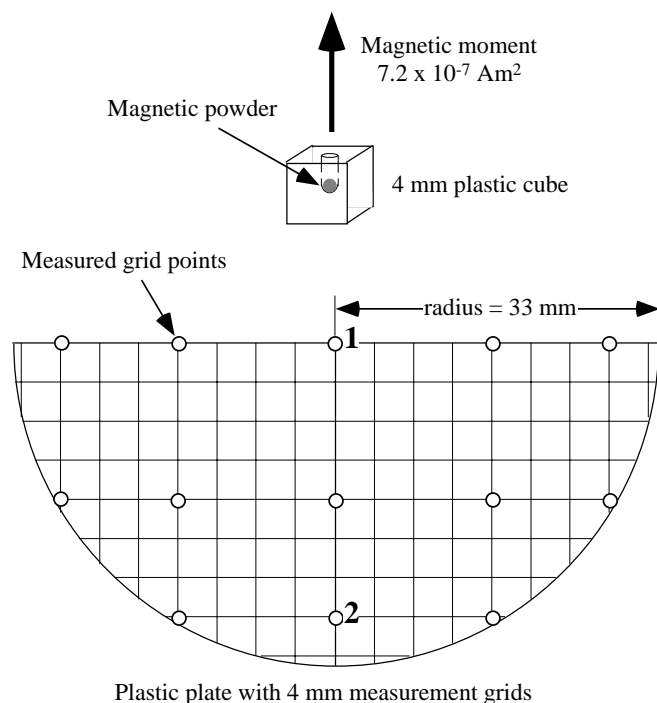


Figure 8. The standard 4-mm cube sample for the sensor-response measurements with stable magnetic moment of  $7.2 \times 10^{-7} \text{ Am}^2$  normal to one face of the cube (upper), and a plastic plate with 4-mm grid marks for measurement of the archive-half samples (lower). Sensor-response measurements were conducted at 5-mm intervals in X, Y, and Z directions successively on the grid points marked with small circles. Numbers 1 and 2 are the points where the sensor responses are shown in Figure 9.

Standard precautions were taken during handling, processing, and extraction (e.g., Mountain, Miller, Blum, et al., 1994). Deviations from the standard ODP sampling scheme are given in the separate site chapters. Chloride, salinity (by refractive index), alkalinity, pH, sulfate, ammonium, dissolved silica ( $\text{H}_4\text{SiO}_4$ ), and phosphate ( $\text{HPO}_4^{2-}$ ) were analyzed according to the methods described in ODP Technical Note No. 15 (Gieskes et al., 1991). Potassium, calcium, and magnesium were analyzed by ion chromatography using a DX-100 ion chromatograph fitted with a CS12 column. Strontium was analyzed by atomic absorption spectroscopy using an air/nitrous oxide flame and 1% lanthanum as an ionization suppressor. The precisions of the methods are given in Table 3.

## ORGANIC GEOCHEMISTRY

Shipboard organic geochemistry for Leg 174A included three routine sets of analyses: (1) volatile hydrocarbon content of gas, (2) inorganic carbon content of sediment, and (3) total carbon, total nitrogen, and total sulfur content of sediment. Organic geochemistry on the leg also included limited Rock-Eval characterization of sediment organic matter. Procedures and instruments used during Leg 174A are described by Ermeis and Kvenvolden (1986) and generally are the same as those used during recent ODP legs. Brief comments on routine sampling and deviations from standard practice are noted below; more detailed notes are presented in the "Explanatory Notes" chapters, ODP Legs 150, 156, and 164 (Shipboard Scientific Party, 1994, 1995c, 1996b).

### Hydrocarbon Gases

Composition of gases in sediment typically was determined at least once every core. Two sampling methods were employed: head-

space sampling (HS) and syringe or void sampling (VS). HS is gas collection after heating a known quantity of sediment in a vial. VS is direct extraction of gas from voids in recovered core. VS on ODP Leg 174A is analogous to (and has replaced) the vacutainer method commonly used during previous ODP legs.

Gas obtained by either method was analyzed by one of two gas chromatography systems: a Hewlett Packard 5890 Series II (GC3), or a Hewlett-Packard 5890A Natural Gas Analyzer (NGA). The first system determines concentrations of  $\text{C}_1$  through  $\text{C}_3$  hydrocarbons with a flame ionization detector (FID); the latter system measures concentrations of  $\text{C}_1$  through  $\text{C}_7$  hydrocarbons with an FID as well as  $\text{N}_2$ ,  $\text{O}_2$ , and  $\text{CO}_2$  with a thermal conductivity detector (TCD). For both systems, chromatographic response was calibrated to six different gas standards with variable quantities of low molecular weight hydrocarbons,  $\text{N}_2$ ,  $\text{O}_2$ ,  $\text{CO}_2$ , Ar, and He.

### Inorganic Carbon and Carbonate

Inorganic carbon content of sediment samples was determined by coulometry. Carbonate content of sediment (in weight percent) was calculated from inorganic carbon (IC) content by assuming all carbonate occurs as calcium carbonate:

$$\text{CaCO}_3 = \text{IC} \times 8.33.$$

### Elemental Analyses

Total carbon, nitrogen, and sulfur contents of sediment samples were determined with a Carlo Erba NCS analyzer. Total organic carbon (TOC) content was calculated as the difference between total carbon (TC) and IC:

$$\text{TOC} = \text{TC} - \text{IC}.$$

### Organic-Matter Characterization

Type and quantity of organic matter in sediment were evaluated by Rock-Eval pyrolysis. In this procedure, volatile hydrocarbon content (mg/g) released at  $300^\circ\text{C}$  for 3 min is  $\text{S}_1$ . Hydrocarbon quantity (mg/g) released as the temperature is increased from  $300^\circ\text{C}$  to  $600^\circ\text{C}$  at  $25^\circ\text{C}/\text{min}$  is  $\text{S}_2$ .  $\text{CO}_2$  (mg/g) released between  $300^\circ\text{C}$  and  $390^\circ\text{C}$  is  $\text{S}_3$ . The nominal temperature of maximum rate of hydrocarbon yield during  $\text{S}_2$  analysis is  $T_{\text{max}}$ . TOC was calculated from  $\text{S}_1$ ,  $\text{S}_2$ , and  $\text{S}_3$ , and from oxidizing remaining carbon in a sediment sample. The carbon-normalized Hydrogen Index (HI,  $\text{mgHC}/\text{gC}$ ) and Oxygen Index (OI,  $\text{mgCO}_2/\text{gC}$ ) were calculated from pyrolysis values:

$$\text{HI} = (100 \times \text{S}_2) / \text{TOC}, \text{ and}$$

$$\text{OI} = (100 \times \text{S}_3) / \text{TOC}.$$

## PHYSICAL PROPERTIES

### Introduction

Shipboard measurements of physical properties aid in the characterization of lithologic units and help correlate core lithology, down-hole geophysical logs, and seismic data. Wet bulk density, compressional wave velocity, magnetic susceptibility, and natural gamma (NGR) were measured in whole-round core sections on the MST (see below). Thermal conductivity measurements using the needle probe method were performed at discrete intervals, also in whole-round sections. Physical properties measurements made on undisturbed sections of split cores included compressional wave velocity, index properties, undrained shear strength, and resistivity. Most samples were extracted at regularly spaced intervals, although some were taken in thin lithologic units that would have been missed by regular

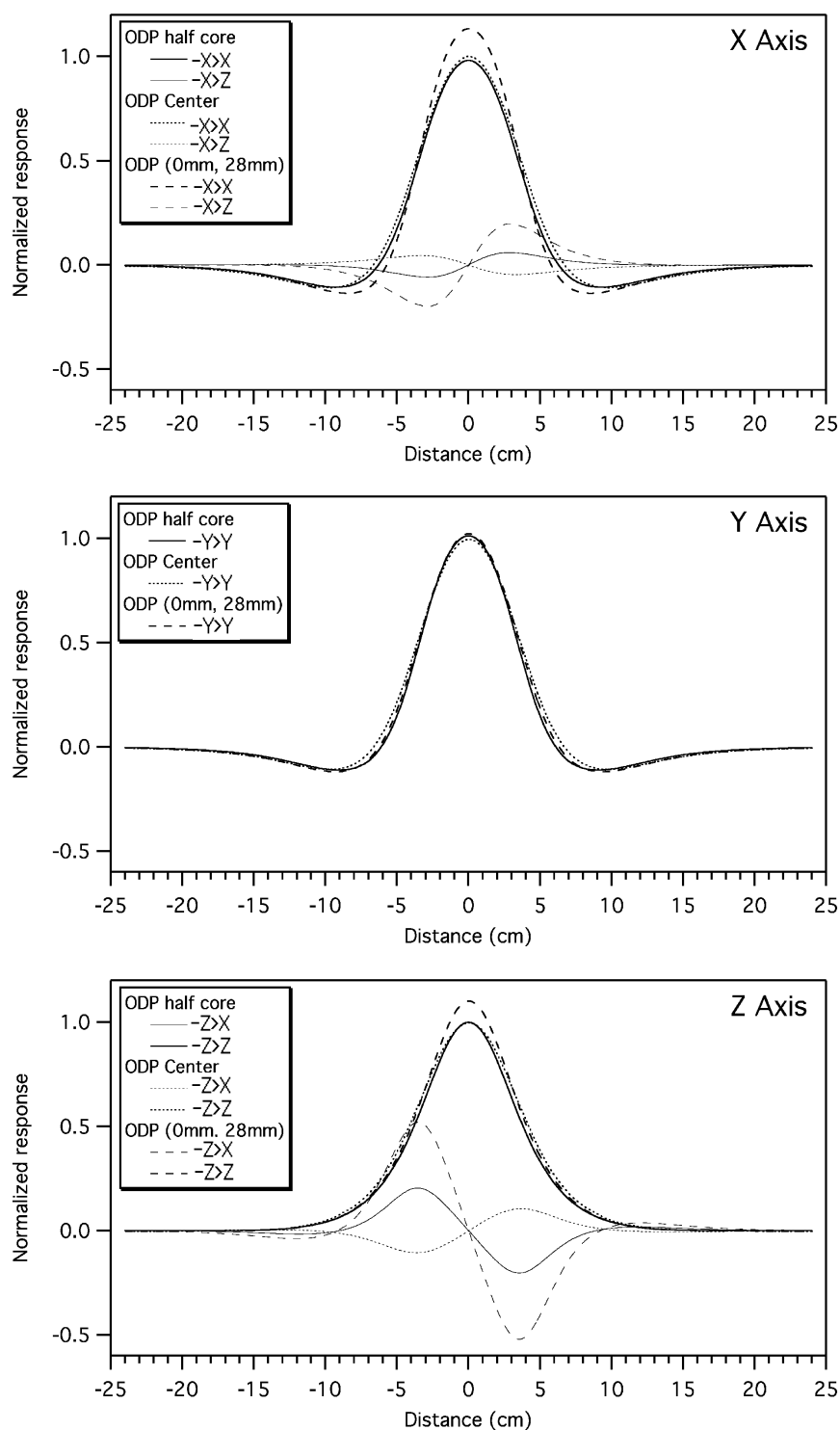


Figure 9. Normalized sensor-response curves for the cryogenic magnetometer for archive-half samples (solid lines) together with response curves measured at the center (dotted lines; Position 1 in Fig. 8) and 28 mm below the center (dashed lines; Position 2 in Fig. 8). Each thick line  $-X>X$ ,  $-Y>Y$ , or  $-Z>Z$  indicates the sensor-response curves for X, Y, or Z magnetization to the X, Y, or Z sensor pick-up coil. Thin line  $-X>Z$  ( $-Z>X$ ) shows the cross term of X (Z) magnetization to Z (X) pick-up coil. Distance is measured from the center of the sensor pick-up coils in the direction of the AF demagnetizer (toward the bow of *JOIDES Resolution*).

sampling patterns. Blum (1997) gives detailed descriptions of most of the techniques used.

### Multisensor Track (MST)

Core sections were run through the MST after they had warmed up to at least 18°C (measured at the top of the section). The gamma-ray attenuation porosity evaluator (GRAPE) measured wet bulk density at 4-cm intervals by comparing the attenuation of gamma rays through the cores with attenuation through aluminum and distilled water calibration standards (Boyce, 1976). GRAPE data are most re-

liable in undisturbed cores; they offer the potential for direct correlation with downhole bulk density logs. However, for discontinuous, fragmented cores with incompletely filled core liners, GRAPE acquisition was turned off.

The *P*-wave logger (PWL) transmits a 500-kHz compressional wave pulse through the core. The transmitting and receiving transducers are aligned perpendicular to the long axis of the core (*y*-direction). A pair of displacement transducers monitors the separation between the compressional wave transducers. As with the GRAPE sensor, measurements were taken at 4-cm intervals, and only continuous cores that filled their core liners were measured. The PWL is the

**Table 3. Relative standard deviations for analysis of dissolved species during Leg 174A.**

Parameter	SD (%)	Sample type
Cl <sup>-</sup>	0.17	IAPSO
Alkalinity	2.8	IAPSO
SO <sub>4</sub> <sup>2-</sup>	1.5	IAPSO
K <sup>+</sup>	2.6	IAPSO
Mg <sup>2+</sup>	1.9	IAPSO
Ca <sup>2+</sup>	3.9	IAPSO
Sr <sup>2+</sup>	2.9	IAPSO
NH <sub>4</sub> <sup>+</sup>	4.9	Standard curve (0.5-30 μM)
HPO <sub>4</sub> <sup>2-</sup>	3.4	Standard curve (1-40 μM)
H <sub>4</sub> SiO <sub>4</sub>	1.2	Standard curve (100-1000 μM)

Notes: SD = standard deviation. IAPSO = International Association for the Physical Sciences of the Ocean.

MST device most sensitive to core condition and was the first to be turned off if core condition deteriorated. Data quality was assessed by examining arrival times and amplitudes of the received pulses. Calibration of the displacement transducer and measurement of electronic delay within the PWL circuitry were performed using a series of acrylic blocks of known thickness and *P*-wave traveltime. The validity of the calibration was checked by measuring the *P*-wave velocity through a section of liner filled with distilled water.

Magnetic susceptibility aids in the detection of fine variations in magnetic intensity associated with magnetic reversals and lithologic changes. It was measured on all sections at 4-cm intervals using a Bartington meter (Model MS2C), which has an 80-mm internal-diameter loop. The quality of these results is degraded if the core liner is not completely filled and/or the core is disturbed. However, general downhole trends may still be used for core to well-log correlation.

NGR was measured at 20-cm intervals in each section, with a counting period of 30 s. The installation and operating procedures for the NGR system are discussed by Hoppie et al. (1994). No corrections were made to XCB-core NGR data to account for sediment incompletely filling the core liner.

### Thermal Conductivity

Thermal conductivity is the measure of a material's ability to transmit heat by molecular conduction. Thermal conductivity of soft sediment was measured using the needle probe method, in full-space configuration (von Herzen and Maxwell, 1959). One measurement per core was made, usually near the middle of the core, using a single-probe TeKa (Berlin) TK-04 unit after the cores had equilibrated to laboratory temperature. Thermal conductivity measurements were made near the bases of cores on which the Adara temperature tool had been run. Data are reported in units of W/(m·K).

A needle probe (#V00894), containing a heater wire and a calibrated thermistor, was inserted into the sediment through a small hole drilled in the core liner, usually near the center of the section, before core splitting. Three measuring cycles were automatically performed at each location. At the beginning of each test, a self-test, which included a drift study, was conducted. Once the samples were equilibrated, the heater circuit was closed, and the temperature rise in the probes was recorded. Thermal conductivities were calculated from the rate of temperature rise while the heater current was flowing.

Temperatures measured ~150 s from the beginning of the run were fitted to an approximate solution of a constantly heated line source (Kristiansen, 1982; see Blum, 1997, for details). Errors are between 5% and 10%. Corrections were not attempted for in situ temperature or pressure effects. Measurements accompanied during processing by "high drift" or "high error" messages were discarded before plotting the results.

### Index Properties

Index properties (bulk density, grain density, water content, porosity, dry density, and void ratio) were calculated from measurements of wet and dry masses and dry volumes. Index property samples of ~10 cm<sup>3</sup> were usually taken at the locations of velocity and resistivity measurements. Sample frequency was increased after Hole 1071A to two per section, when it became apparent that the core flow would not be as high as had been anticipated at shelf sites. Sample frequency was subsequently reduced at high-recovery slope Site 1073.

Sample mass was determined using a Scitech electronic balance. The sample mass was counterbalanced by a known mass, such that only mass differences of usually <2 g were measured. The balance was also equipped with a computer averaging system that corrected for ship accelerations. Dry mass was measured from samples oven dried at 110°C ± 5°C for 24 hr and cooled in a desiccator for 2 hr.

Dry volumes were determined using a Quantachrome Penta-Pycnometer, a helium-displacement pycnometer. Sample volumes were repeated up to three times until the last three measurements had <0.01% standard deviation. A purge time of 1 min was used before each run. A reference sphere of known volume was run with each group of four samples during all the measurements. The standard was rotated systematically among cells to check for errors.

Water content, bulk density, porosity, grain density, dry density, and void ratio were determined following procedures outlined in Blum (1994), which comply with the American Society for Testing and Materials (ASTM) designation (D) 2216 (ASTM, 1989). Bulk density, grain density, and porosity were computed from the wet and dry masses of the sample and dry volume using "method C" of Blum (1994). Calculated values include a correction for salt assuming a pore-water salinity of 35 g/L (Boyce, 1976). However, some pore water is significantly less saline (see "Inorganic Geochemistry" sections of the site chapters, this volume).

### Compressional Wave Velocity

In addition to the velocity measurements with the PWL, compressional wave velocity was measured on split-core sections. Measurement frequency was the same as that for index properties. The pair of transducers measuring velocity along the core axis (PWS1, z-direction) was inserted into soft sediments (orientations of x, y, and z directions are indicated in Shipboard Scientific Party [1996a], Fig. 8). Velocity calculation was based on the fixed distance between the transducers, measurement of the traveltime of an impulsive acoustic signal, and a delay constant determined by measuring a water standard. Periodically, a calibration was performed using distilled water. PWS2, which measures velocity across the width of the split core (y-direction) using similar transducers to PWS1, was not used because it would have disturbed the interval between the PWS1 transducers, where PWS3 (see below) and resistivity measurements (as well as index properties) were generally taken.

A modified Hamilton frame velocimeter measured traveltime of a 500-kHz signal orthogonally across the split-core section and core liner (PWS3, x-direction). Sample thickness was measured directly from the velocimeter/frame through a linear resistor output to a digital multimeter. Delay times for the velocity transducers were estimated by linear regression of traveltime vs. distance for a series of aluminum and lucite standards.

Use of PWS1 was discontinued in more indurated sediments, when sediment started to crack during insertion of the transducers. PWS3 then provided the only velocity measurements. Velocity data recorded in the JANUS database are uncorrected for in situ temperature and pressure (such corrections can be made using relationships in Wyllie et al., 1956; Wilson, 1960; and Mackenzie, 1981).

## Shear Strength

Undrained shear strength ( $S_u$ ) was determined parallel to bedding in fine-grained, plastic sediment using a motorized miniature vane shear device following the procedures of Boyce (1977). The vane rotation rate was set to 90°/min. Measurements were made only in fine-grained, soft to very stiff units. Shear strength was measured at varying intervals, up to twice per section. A range of previously calibrated springs of various strengths was available. The instrument measures the torque and strain at the vane shaft using a torque transducer and potentiometer, respectively. The shear strength reported is the peak strength determined from the torque vs. strain plot. The residual strength was not routinely determined.

In the analyses of vane tests, the assumption is made that failure occurs in an undrained condition on a right circular cylinder equal in surface area to the cylinder inscribed in the sediments by the vane during one continuous revolution, with cohesion as the principal contributor to shear strength. Departures from this assumption include progressive cracking within and outside of the failing specimen, uplift of the failing core cylinder, drainage of local pore pressures (i.e., the test can no longer be considered to be undrained), and stick-slip behavior. Evidence of cracking is noted in the comments section of the results file.

A pocket penetrometer was used when the sediment was neither too soft nor too brittle. The penetrometer is a flat-footed, cylindrical probe that is pushed 6.4 mm into the split-core surface. The penetrometer is calibrated as an unconfined compression test, which (for the ideal clay) measures twice the undrained shear strength, or  $2S_u$  (Holtz and Kovacs, 1981). The mechanical scale is converted into units of kPa by

$$2S_u \text{ (kPa)} = 2S_u \text{ (kg/cm}^2\text{)} \times 98.1 \text{ [kPa/(kg/cm}^2\text{)]}.$$

The maximum  $S_u$  that can be measured with the pocket penetrometer is 220 kPa. Penetrometers are designed for use in soft sediment, and readings were discarded if the sediment cracked during measurement.

## Electrical Resistivity

The Wayne-Kerr Precision Component Analyzer was used to measure resistivity by a four-electrode method, where two outer electrodes inject an alternating current, while two inner electrodes measure the resulting potential difference. The apparent resistance is proportional to the resistivity of the medium. The probes used during Leg 174A consisted of four needles (Wenner array) spaced at 10-mm intervals. Electrical resistivity was generally measured once or twice per section, usually at the locations of velocity and index properties measurements. Additional resistivity measurements were made near locations where interstitial water samples were taken.

The instrument was calibrated using seawater: the area/length parameter of the probe is determined as the ratio of known resistance of seawater at a given temperature to that measured by the probe. The area/length function was determined as 0.061 for the z direction at 15-kHz alternating current frequency. Measurements were primarily in the longitudinal (z) direction only. Some transverse (y direction) resistivity measurements were also made at Site 1073. When both were made, transverse and longitudinal resistivity measurements were made at the same location. It is essential that measurements be made with the same alternating current frequency as used during calibration, because frequency greatly affects measured resistance, so a frequency of 15 kHz was used during Leg 174A. Resistivity of the seawater standard was occasionally measured between measurements on cores to check calibration (see also Shipboard Scientific Party, 1995c).

## DOWNHOLE LOGGING

### Introduction

Downhole logs measure physical and chemical properties of formations adjacent to the borehole. Interpretation of these continuous, in situ measurements yields a mineralogic, lithologic, stratigraphic, and geophysical characterization of the formation adjacent to the borehole wall. Where core recovery is incomplete, log data may serve as a proxy for physical properties and lithology. The principal goals of well logging during Leg 174A were to: (1) provide the depth-traveltime ties between borehole data and seismic reflection profiles, (2) identify lithologic and facies trends within the stratigraphic successions and locate stratigraphic breaks such as sequence and parasequence boundaries, and (3) provide continuous lithologic and petrophysical data to complement the sequence-stratigraphic analysis of the section cored. A combination of wireline and logging-while-drilling (LWD) borehole logs was planned for each site. Acoustic logs in unconsolidated formations ( $V_p < \sim 2$  km/s) can be obtained only through wireline logging. LWD, while it does not offer sonic measurements, offers the advantage of measurements in the upper portion of the boreholes and increases the potential for obtaining high-quality data in unstable formations unsuitable for wireline logging.

### Wireline Logging

To prepare for logging operations after coring was completed, the boreholes were flushed of debris by circulating a “pill” of viscous drilling fluid (sepiolite mud mixed with seawater, approximate weight 8.8 lb/gal or 1.11 kg/m<sup>3</sup>) through the drill pipe to the bottom of the hole. The bottom-hole assembly (BHA) was pulled up to a depth of between 30 and 90 mbsf, and then run down to the bottom of the hole again to ream borehole irregularities. The hole was subsequently filled with sepiolite mud, and the pipe was raised again to 30–90 mbsf. Tool strings comprising one or more combinations of sensors were then lowered downhole by a seven-conductor wireline cable during sequential runs. A wireline heave compensator (WHC) was employed to minimize the effect of ship’s heave on the tool position in the borehole. During each logging run, incoming data were recorded and monitored in real time on the Schlumberger Maxis 500 logging computer. The checkshot well survey used the Well Seismic Tool (WST), and seismic waves were recorded in the Schlumberger Cyber Service Unit (CSU) logging computer.

### Wireline Logging Tool Strings

Four different logging tool combinations were used during Leg 174A: the Integrated Porosity-Lithology Tool string (IPLT or triple-combo), the Formation MicroScanner (FMS) tool string, the Sonic-Resistivity tool string, and the WST. The configuration of these tool strings is shown in Figure 10, together with the measurements obtained by each tool. Each tool string contains a telemetry cartridge at the top of the string, which is used for communication between the surface computer and the downhole tools (telemetry cartridge [TCC] and digital telemetry cartridge [DTC]; see Fig. 10). Below, a brief description of the logging tools employed during Leg 174A is presented; further details can be obtained in the books by Serra (1984), Timur and Toksöz (1985), Ellis (1987), and Schlumberger (1989).

The IPLT string includes the following five logging tools (Fig. 10; Table 4):

1. *Hostile-environment Natural Gamma-ray Spectrometry (HNGS) tool.* This tool measures natural radioactivity of the formation using two 12-in-long Bismuth Germanate (BGO) crystals. Concentrations of K, Th, and U are derived from gamma-ray counts in 256 channels covering the energy spectrum from 0.1 to 3 MeV. Total

gamma-ray data may be used to evaluate clay content; spectral gamma-ray data may be used further to determine mineralogy, such as clay, feldspar, glauconite, or other minerals with radioactive components.

2. *Accelerator Porosity Sonde (APS)*. Neutron porosity tools have a source of neutrons and neutron detectors at various positions within the sonde. In the APS, a pulsing neutron generator (minitron) produces a flux of fast, 14-MeV neutrons. The measurement principle involves counting neutrons that arrive at detectors after being slowed by neutron absorbers surrounding the tool. The highest energy loss occurs when neutrons collide with hydrogen (water) nuclei, which have practically the same mass as the neutron. Upon reaching thermal energies (0.025 eV), the neutrons also are captured by the nuclei of chlorine, silicon, boron, and other elements, resulting in a gamma-ray emission. If the hydrogen (i.e., water) concentration is small, as in low-porosity formations, neutrons can travel farther before being captured, and the count rates increase at the detector. The opposite effect occurs when the water content is high. A bow-spring eccentricizer is used to press the tool against the borehole wall and minimize the effects of borehole fluid on the porosity measurement. The combination of an array of neutron detectors and a pulsed neutron generator makes this tool useful for evaluating formation porosity and the presence of large neutron cross-section elements that are usually associated with clay-rich formations.

3. *Hostile-environment Litho-Density Tool (HLDT)*. The density sonde measures the amount of scattering of gamma rays emitted from a radioactive <sup>137</sup>Cs source using two scintillation crystals. Both crystals and source are placed on a shielded skid that is pressed against the borehole wall by a hydraulic arm. The arm also provides a direct

measure of the borehole diameter. The medium energy gamma rays emitted by the source (662 keV) lose energy by interaction with the electrons in the formation by Compton scattering, until they are absorbed through the photoelectric effect (PEF). The number of gamma rays reaching the two vertically spaced detectors yields an energy spectrum for each detector that is directly related to the number of electrons in the formation, which in turn is a measure of the bulk density. Photoelectric absorption occurs when the gamma rays reach a low energy (<150 keV) after being continually scattered by electrons in the formation. Because the PEF depends on the atomic number of the elements in the formation, the magnitude of this measurement is nearly independent of porosity. The PEF values, when used in combination with other logs, can provide an indication of the different types of minerals in the sediments.

4. *Dual Induction Tool (DIT-E)/Spherically Focused Resistivity Log (SFL) Tool*. This tool provides three measurements of electrical resistivity, each with a different depth of investigation and vertical resolution (Table 4). These are deep induction (IDPH), medium induction (IMPH), and shallow spherically focused resistivities (SFLU). The two induction devices transmit high-frequency alternating currents through transmitter coils, creating magnetic fields that induce secondary currents in the formation. These currents produce a new inductive signal, proportional to the conductivity of the formation, which is measured by the receiving coils. The measured conductivities are then converted to resistivity (in units of ohm-meters). The SFL measures the current necessary to maintain a constant voltage drop across a fixed interval, which is a direct measurement of resistivity. Sand grains and hydrocarbons are electrical insulators, whereas ionic solutions such as seawater and clays are

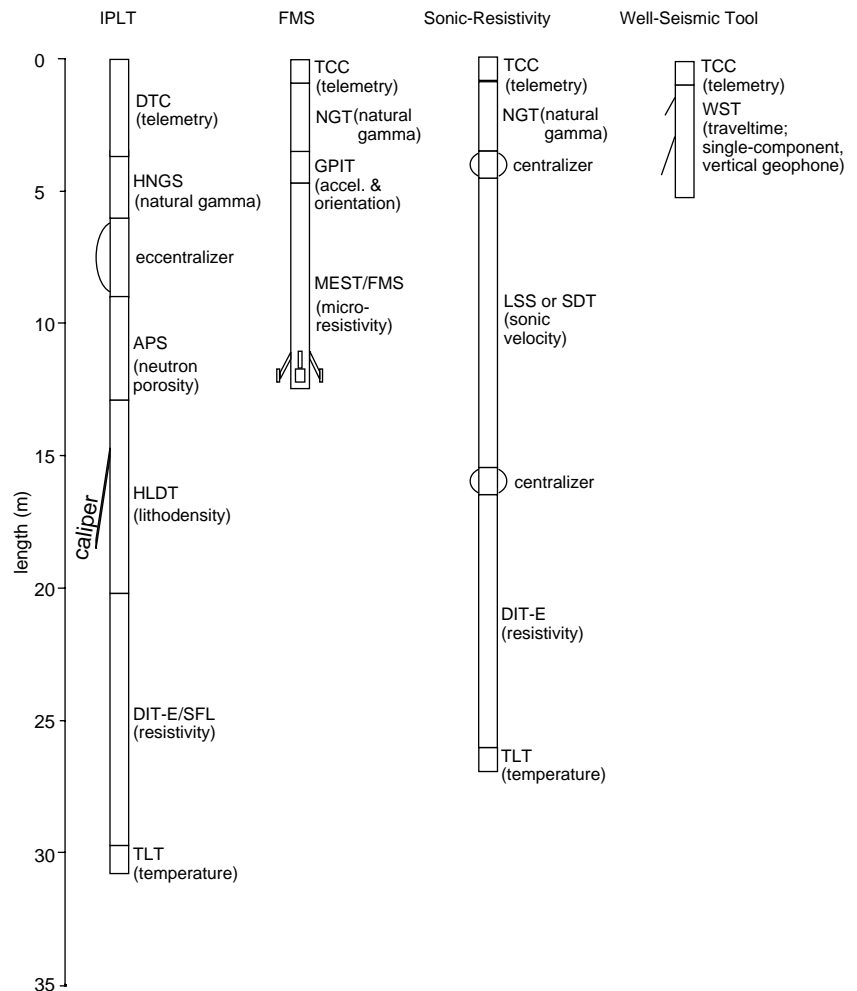


Figure 10. Configuration of tool strings deployed during Leg 174A. DTC and TCC correspond to telemetry cartridges (DTC = digital telemetry cartridge; TCC = telemetry cartridge C); see Table 4 for other acronyms.

**Table 4. Wireline tool strings and acronyms.**

Tool string	Typical speed (m/hr)	Tool	Aim of measurement	Sampling interval (cm)	Approximate vertical resolution (cm)
Integrated Porosity-Lithology Tool (IPLT)	250-275	HNGS	Natural gamma	15	45
		APS	Porosity	3 and 15	30 or 45
		HLDT	Bulk density	5 and 15	10 or 45
		DIT-E/SFL	Resistivity	15	75/150/200
		TLT	Temperature	1 per s	NA
Formation MicroScanner (FMS)	250-275	NGT	Natural gamma	15	45
		GPIT	Orientation	0.25	NA
		MEST/FMS	Microresistivity	0.25	3
Sonic-Resistivity	250-275	NGT	Natural gamma	15	45
		LSS or SDT	Sonic velocity	15	60
		DIT-E	Resistivity	15	75/150/200
		TLT	Temperature	1 per s	NA
Checkshot survey tool string (Well Seismic Tool)	Stationary	WST	Traveltime Source: Generator-injector air-gun (45-105 in <sup>3</sup> )	2000-5000	NA

Notes: Tool acronyms, followed by basic measurements and respective units in parenthesis, are listed here. HNGS = Hostile-environment Natural Gamma-ray Spectrometry tool. NGT = Natural Gamma-ray Tool (SGR [gAPI] = total spectral gamma-ray, CGR [gAPI] = computed uranium-free gamma-ray, and K [wt%], Th [ppm] and U [ppm]). APS = Accelerator Porosity Sonde (APSC [%] = APS near/array sandstone-corrected porosity, FPSC [%] = APS near/far sandstone-corrected porosity, SIGF [capture units] = formation capture cross-section, and STOF [in] = estimated tool stand-off). HLDT = Hostile-environment Litho-Density Tool (RHOB [g/cm<sup>3</sup>] = bulk density, PEF [barns/e<sup>-</sup>] = photoelectric factor, DRHO [g/cm<sup>3</sup>] = Delta-rho, and CALI [in] = hole diameter). DIT-E/SFL = dual induction tool/spherically focused resistivity log (IDPH [Ωm] = phasor-induction deep resistivity, IMPH [Ωm] = phasor induction medium resistivity, and SFLU [Ωm] = shallow spherically focused resistivity). LSS = long-spaced sonic or SDT = digital sonic tool (DT [μs/ft.] =  $V_p$  transit time). GPIT = general purpose inclinometry tool (DEVI [°] = hole deviation, HAZI [°] = hole azimuth, P1AZ [°] = Pad1 azimuth, C<sub>1</sub>/C<sub>2</sub> [in] = orthogonal hole diameters, FCAX, FCAY, FCAZ [m/s<sup>2</sup>] = tool acceleration vector components, and FX, FY, FZ [oersted] = total magnetic field vector components). MEST/FMS = microelectrical resistivity tool or Formation MicroScanner (spatially oriented borehole wall resistivity image). WST = Well Seismic Tool. NA = not applicable.

good conductors. Electrical resistivity can therefore be used to evaluate fluid salinity, water saturation, porosity, and the extent of pore connectivity.

5. *Temperature-Logging Tool (TLT)*. The TLT contains two thermistors and one pressure transducer housed in a pressure case that is placed at the bottom of the IPLT and sonic-resistivity tool strings. Temperature and pressure are recorded once per second and stored in memory. Tool depth as a function of time is recorded at the surface and merged with the temperature vs. time data downloaded from the tool memory after each run. Whereas deployment time usually is short with respect to the time necessary for borehole fluid to reach thermal equilibrium with the formation, the tool can detect temperature anomalies associated with fluid advection into or out of the formation at discrete levels.

The FMS tool string contains two tools (Fig. 10; Table 4):

1. *Natural Gamma-ray Tool (NGT)*. This tool performs the same measurement as the HNGS tool, but uses a single, 12-in-long, sodium iodide (NaI) crystal instead of BGO crystals. The HNGS tool provides statistically more stable spectral estimates, but at this time the tool cannot be combined with the FMS tool string. The total gamma-ray measurements obtained by the NGT in this tool string are used primarily for correlation between different FMS logging runs and between this and other tool string runs.

2. *Formation MicroScanner (FMS)*. The FMS produces high-resolution images of the microresistivity character of the borehole wall. This tool comprises four orthogonal pads, with 16 button electrodes (each 6.7 mm in diameter) on each pad, that are pressed against the borehole wall (Serra, 1989). The electrodes are arranged in two diagonally offset rows of eight electrodes each. Each pad measures ~8 cm<sup>2</sup>; one pass of the tool covers ~30% of a 25-cm diameter borehole. Each individual electrode emits a focused current into the formation. The current intensity measurements in each button are converted to variable intensity color images that indicate microresistivity variations. Processing corrects the offset rows to one level, providing a vertical resolution of a few centimeters (depending on resistivity contrast) and a sampling interval of 0.25 cm (Serra, 1989). The FMS tool also contains a general purpose inclinometer (GPIT) that orients the resistivity measurements through the use of a three-axis accelerometer and a three-axis magnetometer. The electrical borehole images

provide information on fine-scale bedding and sedimentary structures and orientation of geologic features such as bedding, scouring, cross-bedding (and cross-lamination in some instances) and fractures.

### Sonic-Resistivity Tool String

Sound velocity is related to sediment porosity and lithification and/or compaction. In conjunction with density logs or core physical properties measurements, sonic logs are used to compute synthetic seismograms.

The Sonic-Resistivity tool string combines three logging tools in addition to the memory temperature tool (TLT) at the bottom of the string. The string includes the NGT at the top, followed by a sonic tool and the DIT-E tool. Two sonic tools were employed during Leg 174A, the array-sonic tool (SDT) and the Long-Spaced Sonic tool (LSS). Results from the first logging run with the SDT indicated that the tool did not perform well in the relatively slow formations encountered. Following the first logging run, the SDT was replaced with the LSS, with better results. Both sonic tools are briefly described below.

The LSS has two acoustic transmitters spaced 2 ft (61 cm) apart located 8 ft (244 cm) below two acoustic receivers also spaced 2 ft apart. This geometry provided for eight different transit times to be measured, from which one can estimate the sound velocity through the formation, using the multiple time estimates to compensate for noise and borehole irregularities.

The SDT also has a pair of receivers (2 ft spacing) located 3 ft above a pair of transmitters (2 ft spacing). The main difference is that the SDT contains an additional array of eight wideband receivers located 8 ft above the transmitters. These receivers provide for increased spatial sampling of the wavefield and estimation of shear and Stoneley-wave velocities through the formation.

Checkshot well surveys were performed using the Well-Seismic Tool (WST) (Fig. 10). The goal of this seismic experiment was to determine exact depth-time correlations at as many discrete positions in the borehole as possible. The WST consists of a single geophone that is pressed against the borehole wall to record the acoustic waves generated by a source located near the sea surface. We employed a 45/105-in<sup>3</sup> generator-injector (GI) air gun placed at a depth of 2.1 mbsl, offset 48.5 m from the hole on the port side. The WST was clamped

against the borehole wall at intervals of ~30 m, and the GI gun was fired 5–10 times at each clamping position. The resulting waveforms were stacked, and a traveltime was determined from the median of the first breaks in each trace.

Interval transit times also were obtained with the wireline sonic tool (SDT/LSS). However, the acoustic velocities derived from sonic logging usually differ significantly from the seismic velocities used to process the site-survey data (stacking velocities) or checkshot-derived interval velocities because of bad hole conditions, frequency dispersion (e.g., the sonic tool works at 10–20 kHz vs. 10–250 Hz in seismic data), and because the sound is forced to travel along the borehole wall, a path that is quite different from the one taken by the air-gun signal generated during a seismic reflection survey. In addition, sonic logs are not obtained above the BHA, and therefore the traveltime to the uppermost logging point has to be estimated by some other means.

Depth-traveltime pairs determined from the checkshots were used to calibrate the sonic logs and determine accurate drilling depths and their relative position with respect to targets on the seismic reflection profiles. Before Leg 174A drilling, time-depth conversions were estimated from a checkshot survey at the nearby COST-B2 well (Smith et al., 1976) and from stacking velocities measured in the multichannel seismic site-survey data (see “Introduction” chapter, this volume).

### Logging While Drilling

LWD operations have been successfully conducted during three previous ODP legs (Leg 156: Shipley, Ogawa, Blum, et al., 1995; Leg 170: Silver, Kimura, Blum, et al., 1997; and Leg 171A: Moore, Klaus, et al., 1998). LWD logs were provided by Schlumberger-Anadrill Drilling Services under contract with the Lamont-Doherty Earth Observatory-Borehole Research Group (LDEO-BRG). LWD measures in situ formation properties with instruments that are located in the drill collars immediately above the drill bit (Fig. 11). Measurements are made shortly after the hole is cut and before the hole is adversely affected by continued drilling or coring operations. Fluid invasion into the borehole wall also is reduced relative to wireline logging because of the shorter time between drilling and measurement. Unlike wireline logs, LWD can obtain measurements in the top several tens of meters of the borehole. In addition, LWD measurements are made while the drill string is moving, which reduces the risk of the BHA becoming stuck in the hole. LWD measurements were similar to and complemented the wireline measurements made during Leg 174A.

Two Anadrill-Schlumberger LWD tools were combined into the LWD drill string. Figure 11 shows the configuration of the LWD BHA, and Table 5 lists the main set of measurements. The Compensated Dual Resistivity tool (CDR) measures attenuation (deep) and phase shift (shallow) resistivity, and spectral gamma ray; a hole diameter also may be estimated from the phase measurements (PCAL). The Compensated Density Neutron (CDN) tool measures neutron porosity, density, and PEF, as well as a statistically computed differential caliper (DCAL) (Wraight, et al., 1989; Schlumberger, 1993; Desbrandes, 1994; Fig. 11). Measurement principles for the gamma-ray and density tools are similar to the comparable wireline tools, although there are some differences in the measurement parameters. The neutron porosity tool uses an Am-Be source of neutrons instead of the pulsed neutron generator used in the APS, and the LWD source and detector are centered in the borehole rather than being offset like those in the APS. The resistivity tool uses electromagnetic wave propagation at 2 MHz to derive formation resistivity instead of electromagnetic induction in the wireline DIT-E. Although the technology is slightly different because of both the different technological age of the tools and different orientations necessary for different modes of tool deployment, LWD and wireline data are comparable. A more detailed description of the LWD tools and their applications

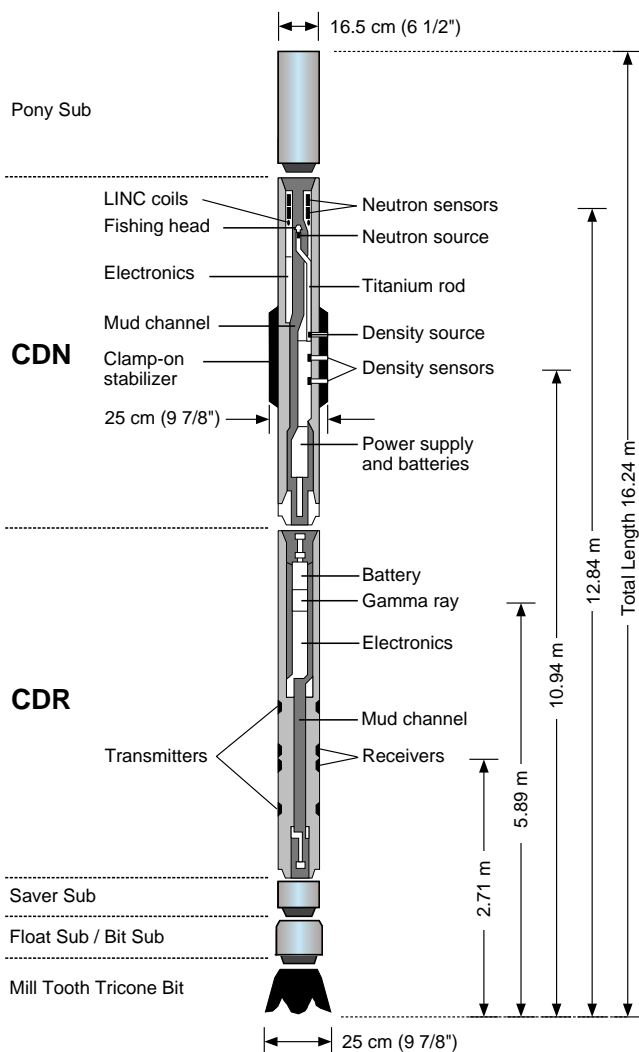


Figure 11. Position and components of Compensated Dual Resistivity (CDR) and Compensated Density Neutron (CDN) tools in the drill string used during Leg 174A logging-while-drilling (LWD) operations.

for ODP may be found in Moore, Klaus, et al. (1998) and Schlumberger (1993).

The LWD equipment is battery powered and uses erasable/programmable, read-only memory (EPROM) chips for nonvolatile data storage during data collection and retrieval. The downhole data acquisition systems are synchronized with a system on the rig that monitors time and drilling depth. For the additional depth control required on the moving ship, three optical-quadrature phase shift encoders were installed on the drilling apparatus to measure drawworks movement, heave compensator stroke, and top drive position (see also Moore, Klaus, et al., 1998). On completion of drilling, the drill string was retrieved and the data downloaded from each tool via a RS232 serial link to a PC computer. During initial shipboard processing, LWD depth data were passed through a low-pass filter to remove the effects of the high-frequency heave, leaving only the true bit movement.

The IDEAL (Integrated Drilling Evaluation and Logging) system combines the files and generates ASCII, log information standard (LIS), and digital log information standard (DLIS) data files. This system also was used for postacquisition data corrections and analyses. Further processing will be conducted postcruise at LDEO-BRG and at other research centers.

**Table 5. Logging-while-drilling tools, acronyms, and measurement specifications.**

6-in sampling interval	ROP*5 = 5-ft averaged rate of penetration (m/hr)
Compensated Dual Resistivity (CDR)	RTIM = resistivity time after bit (s) GTIM = gamma ray time after bit (s) R <sub>ad</sub> = resistivity attenuation deep ( $\Omega$ m) R <sub>ps</sub> = resistivity phase shift shallow ( $\Omega$ m) PCAL = phase caliper (in)
Natural Gamma Tool (NGT; part of CDR)	GR = total gamma ray (GAPI) SGR = total spectral gamma ray (cps) CGR = corrected spectral gamma ray (potassium + thorium; cps) THOR = Thorium (ppm) URAN = Uranium (ppm) POTA = Potassium (wt%)
Compensated Density Neutron (CDN)	DCAL = differential caliper (in) NTAB = neutron time after bit (s) DTAB = density time after bit (s) TNPH = thermal neutron porosity (v/v) PEF = photoelectric effect (barns/e <sup>2</sup> ) ROMT = density (rotationally processed; g/cm <sup>3</sup> ) DRHO = delta-rho (g/cm <sup>3</sup> ) = difference between densities computed from "near" and "far" sensors
3-in sampling interval	CDR = QRO processed data AT1F = attenuation resistivity, 1-ft resolution PS1F = phase shift resistivity, 1-ft resolution
1-in sampling interval	CDN = enhanced vertical resolution processed NROM = resolution enhanced density (actual resolution ~3 in)

## REFERENCES

- ASTM, 1989. *Annual Book of ASTM Standards for Soil and Rock: Building Stones* (Vol. 4.08): *Geotextiles*: Philadelphia (Am. Soc. Testing and Mater.).
- Balsam, W.L., Damuth, J.E., and Schneider, R.R., 1997. Comparison of shipboard vs. shore-based spectral data from Amazon-fan cores: implications for interpreting sediment composition. In Flood, R.D., Piper, D.J.W., Klause, A., Peterson, L.C. (Eds.), *Proc. ODP, Sci. Results*, 155: College Station, TX (Ocean Drilling Program), 193–215.
- Berggren, W.A., Kent, D.V., Swisher, C.C., III, and Aubry, M.-P., 1995. A revised Cenozoic geochronology and chronostratigraphy. In Berggren, W.A., Kent, D.V., Aubry, M.-P., and Hardenbol, J. (Eds.), *Geochronology, Time Scales and Global Stratigraphic Correlation*. Spec. Publ.—SEPM (Soc. Sediment. Geol.), 54:129–212.
- Blow, W.H., 1969. Late middle Eocene to Recent planktonic foraminiferal biostratigraphy. In Brönnimann, P., and Renz, H.H. (Eds.), *Proc. First Int. Conf. Planktonic Microfossils, Geneva, 1967*: Leiden (E.J. Brill), 1:199–422.
- Blum, P., 1994. *Index Properties: ODP Shipboard Laboratory Manual*, Version 155, College Station, TX (Ocean Drilling Program).
- , 1997. Core Physical Properties Measurements on Board the *JOIDES Resolution*, Draft Version, College Station, TX (Ocean Drilling Program).
- Boyce, R.E., 1976. Definitions and laboratory techniques of compressional sound velocity parameters and wet-water content, wet-bulk density, and porosity parameters by gravimetric and gamma-ray attenuation techniques. In Schlanger, S.O., Jackson, E.D., et al., *Init. Repts. DSDP*, 33: Washington (U.S. Govt. Printing Office), 931–958.
- , 1977. Deep Sea Drilling Project procedures for shear strength measurement of clayey sediment using modified Wykeham Farrance laboratory vane apparatus. In Barker, P.F., Dalziel, I.W.D., et al., *Init. Repts. DSDP*, 36: Washington (U.S. Govt. Printing Office), 1059–1068.
- Brinkhuis, H., Powell, A.J., and Zavenboom, D., 1992. High-resolution dinoflagellate cyst stratigraphy of the Oligocene/Miocene transition interval in north-west and central Italy. In Head, M.J., and Wrenn, J.H. (Eds.), *Neogene and Quaternary Dinoflagellate Cysts and Acritarchs*. Am. Assoc. Stratigr. Palynol. Found., 219–258.
- Buck, K.F., and Olson, H.C., in press. *Elphidium* faunas of the New Jersey shelf: implications for sea-level fluctuations during late Quaternary glaciation. *J. Foraminiferal Res.*
- Bukry, D., 1973. Low-latitude coccolith biostratigraphic zonation. In Edgar, N.T., Saunders, J.B., et al., *Init. Repts. DSDP*, 15: Washington (U.S. Govt. Printing Office), 685–703.
- , 1975. Coccolith and silicoflagellate stratigraphy, northwestern Pacific Ocean, Deep Sea Drilling Project Leg 32. In Larson, R.L., Moberly, R., et al., *Init. Repts. DSDP*, 32: Washington (U.S. Govt. Printing Office), 677–701.
- Chaisson, W.P., and Leckie, R.M., 1993. High-resolution Neogene planktonic foraminifer biostratigraphy of Site 806, Ontong Java Plateau (western equatorial Pacific). In Berger, W.H., Kroenke, L.W., Mayer, L.A., et al., *Proc. ODP, Sci. Results*, 130: College Station, TX (Ocean Drilling Program), 137–178.
- Cushman, J.A., and Cahill, E.D., 1933. Foraminifera of the coastal plain of the Eastern U.S. *Geol. Surv. Prof. Pap. U.S.*, 175A.
- de Verteuil, L., and Norris, G., 1996. Miocene dinoflagellate stratigraphy and systematics of Maryland and Virginia. *Micropaleontology*, 42 (Suppl.).
- Desbrandes, R., 1994. *Data Acquisition and Processing While Drilling*. Dept. Petrol. Eng., Louisiana State Univ.
- Droser, M.L., and Bottjer, D.J., 1991. Trace fossils and ichnofabric in Leg 119 cores. In Barron, J., Larsen, B., et al., *Proc. ODP, Sci. Results*, 119: College Station, TX (Ocean Drilling Program), 635–641.
- Ellis, D.V., 1987. *Well Logging for Earth Scientists*: New York (Elsevier).
- Ellison, R.L., and Nichols, M.N., 1976. Modern and Holocene foraminifera in the Chesapeake Bay region. In Schafer, C.T., and Pelletier, (Eds.), *First International Symposium on Benthonic Foraminifera of Continental Margins*, (Pt. A). Maritime Sediment., Spec. Publ., 1:131–151.
- Emeis, K.-C., and Kvenvolden, K.A., 1986. Shipboard organic geochemistry on *JOIDES Resolution*. *ODP Tech. Note*, 7.
- Gevirtz, J.L., Park, R.A., and Friedman, G.M., 1971. Paraecology of benthonic Foraminifera and associated micro-organisms of the continental shelf off Long Island, New York. *J. Paleontol.*, 45:153–177.
- Gibson, T.G., 1983. Key foraminifera from upper Oligocene to lower Pleistocene strata of the central Atlantic coastal plain. *Smith. Contrib. Paleobiol.*, 53:354–453.
- Gieskes, J.M., Gamo, T., and Brumsack, H., 1991. Chemical methods for interstitial water analysis aboard *JOIDES Resolution*. *ODP Tech. Note*, 15.
- Harland, R., 1992. Dinoflagellate cysts of the Quaternary System. In Powell, A.J. (Ed.), *A Stratigraphic Index of Dinoflagellate Cysts*. Br. Micropaleontol. Soc. Publ. Ser.: London (Chapman Hall).
- Head, M.J., and Norris, G., 1989. Palynology and dinocyst stratigraphy of the Eocene and Oligocene in ODP Leg 105, Hole 647A, Labrador Sea. In Srivastava, S.P., Arthur, M.A., Clement, B., et al., *Proc. ODP, Sci. Results*, 105: College Station, TX (Ocean Drilling Program), 515–550.
- Head, M.J., Norris, G., and Mudie, P.J., 1989. Palynology and dinocyst stratigraphy of the Miocene in ODP Leg 105, Hole 645E, Baffin Bay. In Srivastava, S.P., Arthur, M.A., Clement, B., et al., *Proc. ODP, Sci. Results*, 105: College Station, TX (Ocean Drilling Program), 467–514.
- Holtz, R.D., and Kovacs, W.D., 1981. *An Introduction to Geotechnical Engineering*: Englewood Cliffs, NJ (Prentice-Hall).
- Hoppie, B.W., Blum, P., and the Shipboard Scientific Party, 1994. Natural gamma-ray measurements on ODP cores: introduction to procedures with examples from Leg 150. In Mountain, G.S., Miller, K.G., Blum, P., et al., *Proc. ODP, Init. Repts.*, 150: College Station, TX (Ocean Drilling Program), 51–59.

- Kennett, J.P., and Srinivasan, M.S., 1983. *Neogene Planktonic Foraminifera: A Phylogenetic Atlas*: Stroudsburg, PA (Hutchinson Ross).
- Kristiansen, J.I., 1982. The transient cylindrical probe method for determination of thermal parameters of earth materials [Ph.D. dissert.] Dep. Geol., Aaehus Univ., *Geoskrifter*, 18.
- Loeblich, A.R., Jr., and Tappan, H., 1953. Studies of Arctic Foraminifera. *Smithson. Misc. Collect.*, 121.
- Mackenzie, K.V., 1981. Nine-term equation for sound speed in the oceans. *J. Acoust. Soc. Am.*, 70:807–812.
- Manheim, F.T., and Sayles, F.L., 1974. Composition and origin of interstitial waters of marine sediments, based on deep sea drill cores. In Goldberg, E.D. (Ed.), *The Sea* (Vol. 5): *Marine Chemistry: The Sedimentary Cycle*: New York (Wiley), 527–568.
- McKee, E.D., and Weir, G.W., 1953. Terminology for stratification and cross-stratification in sedimentary rocks. *Geol. Soc. Am. Bull.*, 64:381–390.
- Miller, K., Rufolo, S., Sugarman, P., Pekar, S., Browning, J., and Gwynn, D., 1997. Early to middle Miocene sequences, systems tracts, and benthic foraminiferal biofacies, New Jersey coastal plain. In Miller, K.G., and Snyder, S.W. (Eds.), *Proc. ODP, Init. Repts.*, 150X: College Station, TX (Ocean Drilling Program), 169–186.
- Moore, J.C., Klaus, A., et al., 1998. *Proc. ODP, Init. Repts.*, 171A: College Station, TX (Ocean Drilling Program).
- Mountain, G.S., Miller, K.G., Blum, P., et al., 1994. *Proc. ODP, Init. Repts.*, 150: College Station, TX (Ocean Drilling Program).
- Mudie, P.J., 1987. Palynology and dinoflagellate biostratigraphy of Deep Sea Drilling Project Leg 94, Sites 607 and 611, North Atlantic Ocean. In Ruddiman, W.F., Kidd, R.B., Thomas, E., et al., *Init. Repts. DSDP*, 94 (Pt. 2): Washington (U.S. Govt. Printing Office), 785–812.
- Munsell Color Company, Inc., 1990. *Munsell Soil Color Charts*: Baltimore, MD (Munsell).
- Murray, J.W., 1969. Recent foraminifera from the Atlantic continental shelf of the United States. *Micropaleontology*, 15:401–419.
- Oda, H., and Shibuya, H., 1996. Deconvolution of long-core paleomagnetic data of Ocean Drilling Program by Akaike's Bayesian Information Criterion minimization. *J. Geophys. Res.*, 101:2815–2834.
- Okada, H., and Bukry, D., 1980. Supplementary modification and introduction of code numbers to the low-latitude coccolith biostratigraphic zonation (Bukry, 1973; 1975). *Mar. Micropaleontol.*, 5:321–325.
- Olsson, R.K., Melillo, A.J., and Schreiber, B.L., 1987. Miocene sea level events in the Maryland Coastal Plain and the offshore Baltimore Canyon Trough. In Ross, C., and Haman, D. (Eds.), *Timing and Depositional History of Eustatic Sequences: Constraints on Seismic Stratigraphy*. Spec. Publ. Cushman Found. Foraminiferal Res., 24:85–97.
- Parker, F.L., 1948. Foraminifera of the continental shelf from the Gulf of Maine to Maryland. *Bull. Mus. Comp. Zool. Harvard Coll.*, 100:213–241.
- Poag, C.W., Knebel, H.J., and Todd, R., 1980. Distribution of modern benthic foraminifera on the New Jersey Outer Continental Shelf. *Mar. Micropaleontol.*, 5:43–69.
- Powell, A.J., 1992. Dinoflagellate cysts of the Tertiary System. In Powell, A.J. (Ed.), *A Stratigraphic Index of Dinoflagellate Cysts*: London (Chapman and Hall), 155–251.
- Schlumberger, 1989. *Log Interpretation Principles/Applications*: Houston, TX (Schlumberger Educ. Services).
- , 1993. *Logging While Drilling*: Houston, TX (Schlumberger Educ. Services), SMP-9160.
- Schneider, R.R., Cramp, A., Damuth, J.E., Hiscott, R.N., Kowsmann, R.O., Lopez, M., Nanayama, F., Normark, W.R., and Shipboard Scientific Party, 1995. Color-reflectance measurements obtained from Leg 155 cores. In Flood, R.D., Piper, D.J.W., Klaus, A., et al., *Proc. ODP, Init. Repts.*, 155: College Station, TX (Ocean Drilling Program), 697–700.
- Schnitker, D., 1970. *Upper Miocene Foraminifera From Near Grimeland, Pitt County, North Carolina*. N.C. Dep. Conserv. Develop., Div. Miner. Resour., Spec. Publ. 3.
- Serra, O., 1984. *Fundamentals of Well-Log Interpretation* (Vol. 1): *The Acquisition of Logging Data*: Dev. Pet. Sci., 15A: Amsterdam (Elsevier).
- , 1989. *Formation MicroScanner Image Interpretation*: Houston (Schlumberger Educ. Services), SMP-7028.
- Shepard, F., 1954. Nomenclature based on sand-silt-clay ratios. *J. Sediment. Petrol.*, 24:151–158.
- Shipboard Scientific Party, 1994. Explanatory notes. In Mountain, G.S., Miller, K.G., Blum, P., et al., *Proc. ODP, Init. Repts.*, 150: College Station, TX (Ocean Drilling Program), 21–42.
- , 1995a. Explanatory notes. In Curry, W.B., Shackleton, N.J., Richter, C., et al., *Proc. ODP, Init. Repts.*, 154: College Station, TX (Ocean Drilling Program), 11–38.
- , 1995b. Explanatory notes. In Flood, R.D., Piper, D.J.W., Klaus, A., et al., *Proc. ODP, Init. Repts.*, 155: College Station, TX (Ocean Drilling Program), 47–81.
- , 1995c. Explanatory notes. In Shipley, T.H., Ogawa, Y., Blum, P., et al., *Proc. ODP, Init. Repts.*, 156: College Station, TX (Ocean Drilling Program), 39–68.
- , 1996a. Explanatory notes. In Jansen, E., Raymo, M.E., Blum, P., et al., *Proc. ODP, Init. Repts.*, 162: College Station, TX (Ocean Drilling Program), 21–45.
- , 1996b. Explanatory notes. In Paull, C.K., Matsumoto, R., Wallace, P.J., et al., *Proc. ODP, Init. Repts.*, 164: College Station, TX (Ocean Drilling Program), 13–41.
- Shipley, T.H., Ogawa, Y., Blum, P., et al., 1995. *Proc. ODP, Init. Repts.*, 156: College Station, TX (Ocean Drilling Program).
- Silver, E., Kimura, G., Blum, P., et al., 1997. *Proc. ODP, Init. Repts.*, 170: College Station, TX (Ocean Drilling Program).
- Smith, M.A., Amato, R.V., Furbush, M.A., Pert, D.M., Nelson, M.E., Hendrix, J.S., Tamm, L.C., Wood, G., Jr., and Shaw, D.R., 1976. Geological and operational summary, COST No. B-2 Well, Baltimore Canyon Trough Area, Mid-Atlantic OCS. *Open-File Rep., U.S. Geol. Surv.*, 76-774.
- Snyder, S.W., Waters, V.J., and Moore, T.L., 1989. Benthic foraminifera and paleoecology of Miocene Pungo River Formation sediments in Onslow Bay, North Carolina continental shelf. In Snyder, S.W. (Ed.), *Micropaleontology of Miocene Sediments in the Shallow Subsurface of Onslow Bay, North Carolina Continental Shelf*. Spec. Publ. Cushman Found. Foraminiferal Res., 25:43–96.
- Stokking, L.B., Musgrave, R.J., Bontempo, D., and Autio, W., 1993. Handbook for Shipboard Paleomagnetists. *ODP Tech. Note*, 18: College Station, TX (Ocean Drilling Program).
- Timur, A., and Toksöz, M.N., 1985. Downhole geophysical logging. *Annu. Rev. Earth Planet. Sci.*, 13:315–344.
- van Morkhoven, F.P.C.M., Berggren, W.A., and Edwards, A.S., 1986. Cenozoic cosmopolitan deep-water benthic foraminifera. *Bull. Cent. Rech. Explor.—Prod. Elf-Aquitaine*, Mem. 11.
- Von Herzen, R.P., and Maxwell, A.E., 1959. The measurement of thermal conductivity of deep-sea sediments by a needle-probe method. *J. Geophys. Res.*, 64:1557–1563.
- Wentworth, C.K., 1922. A scale of grade and class terms of clastic sediments. *J. Geol.*, 30:377–392.
- Williams, G.L., Stover, L.E., and Kidson, E.J., 1993. *Morphology and Stratigraphic Ranges of Selected Mesozoic-Cenozoic Dinoflagellate Taxa in the Northern Hemisphere*. Pap.—Geol. Surv. Can., 92-10.
- Wilson, W.D., 1960. Speed of sound in seawater as a function of temperature, pressure and salinity. *J. Acoust. Soc. Am.*, 32:641–644.
- Wright, P., Evans, M., Marienback, E., Rhein-Knudsen, E.M., and Best, D., 1989. Combination formation density and neutron porosity measurements while drilling. *Trans. SPWLA 30th Ann. Logging Symp.*, Denver.
- Wyllie, M.R.J., Gregory, A.R., and Gardner, L.W., 1956. Elastic wave velocities in heterogeneous and porous media. *Geophysics*, 21:41–70.